Geochronology of monazite related to REE, Nb-Ta and U-Th bearing minerals from Mesoproterozoic anorogenic magmatism in the E-Colombian Amazonian Craton: links to mantle plume activity in the Columbia (Nuna) supercontinent

José Alejandro Franco Victoria, Thomas Cramer, Alexandre de Oliveira Chaves, Heinrich Adolf Horn, Marc Poujol

HAL Id: insu-03150739

https://insu.hal.science/insu-03150739

Submitted on 24 Feb 2021

Geochronology of monazite related to REE, Nb-Ta and U-Th bearing minerals from Mesoproterozoic anorogenic magmatism in the E-Colombian Amazonian Craton: links to mantle plume activity in the Columbia (Nuna) supercontinent

Franco, José Alejandro[1,2]; Cramer, Thomas [1,2], Chaves, Alexandre de Oliveira[3]; Horn, Heinrich Adolf[2,3]; Poujol, Marc[2,4]

1. *Universidad Nacional de Colombia, Bogotá, Colombia. Corresponding author e-mail: jafrancov@unal.edu.co*
2. *Grupo de Estudios en Geología Económica y Mineralogía Aplicada (G.E.G.E.M.A)*
3. *Universidade Federal de Minas Gerais (UFMG), Av. Antonio Carlos 6627, 31.270-901 Belo Horizonte – Brazil*
4. *Univ Rennes, CNRS, Géosciences Rennes-UMR 6118, F-35000 Rennes, France.*

Abstract

U-Th-Pb geochronology of REE-bearing minerals such as monazite and other phosphates has become a precise tool to date mineralization events through geological time. In the E-Colombian Guainía department, from 3 colluvial sites over western Guiana Shield Mesoproterozoic rocks Nb-Ta, U-Th and REE bearing minerals probably of pegmatitic origin were sampled including up-to-0.5 cm long monazite crystals. The monazite pan concentrate samples from sites near to the indigenous communities of Barranquilla, San Jose and Chorro Bocón (Espina hills) along the Cuyari, Guainía, and Inírida rivers respectively, were analyzed geochemically and geochronologically using LA-ICP-MS and EPMA. The monazites obtained from the 3 sites are rather similar among each another and of approximate composition $Ce_{0.44}La_{0.16}Nd_{0.16}Sm_{004}Y_{0.03}Gd_{0.02}Dy_{0.01}Pr_{0.05}Th_{0.08}Pb_{0.01}Ca_{0.05}Si_{0.05}P_{0.91}O_{3.94}$. Their EPMA and LA-ICP-MS ages suggest at least two mineralization events, a first one between 1528 and 1523 Ma in the Barranquilla and San Jose sites, related to rapakivi granites outcropping along the Cuyarí River and the Tabaquen rapakivi granite near the Guainía River, both emplaced ~1545 Ma ago. The second mineralization event from 1390-1343 Ma recorded in the Espina-hills is in the age range of the Matraca and Danta rapakivi granites that crystalized between 1400 and 1340 Ma ago. These different anorogenic rapakivi granites were emplaced between 1550 and 1300 Ma into Mesoproterozoic basement rocks and were probably caused by intra-plate processes associated with mantle plume activity within the Columbia (Nuna) supercontinent.

Key words: monazite; U-Pb and EPMA geochronology; anorogenic magmatism; mantle plume; Columbia (Nuna) supercontinent.

1 Introduction

Due to their high ionic charge and large ionic radii, Rare Earth Elements (REE) are not easily incorporated within the early-crystallizing silicates (Winter, 2001). Instead, they are enriched in highly differentiated magmatic phases together with other incompatible elements (such as P, K, Rb, U, Th). Despite similar chemical properties, they may be partitioned by either geochemical, mineralogical, and petrological processes in which case they become valuable proxies to study them (Henderson, 1984).

Generally spoken, Light Rare Earth Elements (LREE) tend to be concentrated in pegmatites and carbonatites, whereas Heavy Rare Earth Elements (HREE) are concentrated in granitic magmas (Pirajno, 2009).

Monazite is a LREE phosphate with the generalized formula (LnIII, Th) (PO_4), where LnIII represents a trivalent light lanthanide, and is part of a complete solid solution with the LREE from La - Ce to Sm. Although present in most rock types, monazite is frequently found as an accessory mineral in low-Ca igneous rocks (Itano et al., 2016), instead of apatite and/or bastnäsite mineralization, and in differentiated magmatic phases like granites, syenites and granitic pegmatites. As monazite frequently occurs in colluvial and placer deposits, it is often better studied in these types of deposits than in the magmatic phases where they crystallized (Dill, 2010; Dill et al., 2012).

Elemental analyses of monazite can bring some information on its origin. For example, Itano et al. (2018) found that the La/Sm ratios in monazite grains from granite and granitic pegmatite and from magnetite and ilmenite magmas were different. This ratio could therefore be used as a good proxy for the type of magma. Although monazite can contain up to 12 wt% ThO_2 (Mottana et al., 1978) it is never metamict (Seydoux-Guillaume et al., 2018) and, such as zircon, usually does not incorporate initial lead when it crystallizes. Therefore, all the Pb comes from the radioactive decay of Th and U, which makes monazite a mineral suitable for U-Th-Pb dating via EPMA (electron probe micro analysis) (Itano et al., 2016) as described by Montel et al., (1996), Suzuki and Kato (2008) and Chaves et al., (2013). This type of analyses should however be used with caution as, in some cases, EPMA dating can fail to resolve different monazite age populations as demonstrated by Poujol et al. (2017). Their use as geochronometers by means of LA-ICP-MS (Laser ablation inductively coupled plasma mass spectrometry) and EPMA is compiled by Engi (2017) and Williams et al. (2017).

Crustal-melt rapakivi granites with their characteristic coarse zoned feldspar megacrysts in a finer matrix are probably the result of mantle plume activity (Pirajno, 2007). In eastern Colombia, several authors have reported ages between 1550 and 1340 Ma for anorogenic rapakivi granites such as the Parguaza, Danta, Matraca and Tabaquen intrusions (e.g. Bonilla et al., 2013, 2016; Cordani et al., 2016). In these granites, pegmatitic phases may host monazite, xenotime, columbite-tantalite, Nb-rich rutile as well as U oxides.

84 For this research, three localities in the E-Colombian Guainía Department were
85 selected (Figures 1 and 2): Espina hills – near the Inírida river LOC (4), San José
86 – near the Guainía river LOC (5) and Barranquilla – near the Cuyarí river LOC (6)
87 where Mesoproterozoic pegmatite-related colluvial rock fragments contain
88 centimetric Ti, Nb-Ta, U and Th bearing minerals together with monazite and
89 xenotime. Here we present EPMA and LA-ICP-MS analyses performed on
90 monazite crystals in order to determine their elemental compositions as well as
91 their crystallization ages in order to understand their possible provenance within
92 the western Guiana Shield, i.e. the NW-part of the Amazonian Craton.

93 Further we discuss pegmatitic phases with Ti, Nb-Ta, U-Th and REE
94 mineralization in relation to the 1550-1340 Ma anorogenic granites found in
95 various parts of the western Amazonian Craton in the light of intra-plate processes
96 associated with mantle plume activity, which may have controlled this magmatism
97 within the Columbia (Nuna) supercontinent.

98 **2   Methods used**

99 From panning concentrates (pc) more than 20 monazite crystals from each locality
100 were picked and verified using a handheld Bruker Tracer III-V X-ray fluorescence
101 instrument equipped with a Rh-tube and Silicon Drift Detector (SDD), working
102 conditions 15-40kV, 5-10mA, 60-120s exposure time, no filter nor vacuum which
103 together with the S1PXRF software allow to detect all elements heavier than Na
104 (e.g. Magrini et al., 2018). Three epoxy resin pucks, labeled LOC (4), LOC (5) and
105 LOC (6), each with ~10 crystals, were prepared using buehler epoxy cure2 resin
106 and hardener, polished first with silicon carbide and diamond and then coated with
107 graphite (Mange and Wright, 2007; Reed, 2005). Scanning electron microscopy
108 (SEM) BSE images of the monazite crystals allowed choosing the most
109 homogeneous zones, free of inclusions or in very low proportion. Their chemical
110 composition was determined using wavelength-dispersive spectroscopy (WDS) in
111 a JEOL JXA-8900 EPMA in the Laboratory of Microanalysis of the Microscopy
112 Center at Federal University of Minas Gerais (LMA-CM-UFMG), Brazil. The
113 reference materials used were Y_2O_3 (YAG_25K50n), Dy_2O_3 (DyPO$_4$_25K50n),
114 P_2O_5 (Monaz_25K50n), SiO_2 (ThSiO$_4$_25K50n), Gd_2O_3 (GdPO$_4$_25K50n), PbO
115 (Crocoi_25K50n), Sm_2O_3 (REE$_2$_25K50n), ThO_2 (ThSiO4_25K50n), Nd_2O_3
116 (NdPO$_4$_25K50n), UO_2 (UO$_2$_25K50n), Pr_2O_3 (PrPO$_4$_25K50n), CaO
117 (Ca$_2$P$_2$O$_7$_25K50n), (Ce$_2$O$_3$) (Monaz_25K50n) and La_2O_3 (Monaz_25K50n).
118 Additionally, 30 monazite crystals up-to-0,5 cm large from LOC (5) were analyzed.
119 For EPMA dating, from each locality 1 monazite crystal from the polished epoxy
120 pucks was selected, and ages were calculated using U, Th and Pb concentrations
121 (Williams et al., 2007).

122 The EPMA-analyses were performed in 6 to 10 spots per crystal. Standards and
123 quantitative WDS analytical parameters used during monazite analyses are
124 described in Chaves et al. (2013). Overlaps of X-ray peaks between Y and Pb
125 have not been corrected because there was no measurement in PbMa (Lead M

126 alpha), but only in PbMb (Lead M beta). However, to avoid errors in the obtained
127 ages, the interference of ThMz (Thorium M gamma) on the measured UMb
128 (Uranium M beta) had to be corrected, following Scherrer et al. (2000) in
129 adaptation to the conditions of the LMA-CM-UFMG, as follows (Chaves et al.
130 2013):

131 U corrected = U measured − (0.006365 x Th measured).

132 Microprobe chemical U-Th-Pb_T ages and associated errors were obtained using
133 EPMA Dating software (Pommier et al., 2004) and the average ages were taken
134 through Isoplot/Ex software (Ludwig, 2003). The age equation used is:

135 $Pb = \{Th \times [\exp(\lambda232T) - 1] \times (M208 / M232)\} + \{Uc \times [\exp(\lambda238T)$
136 $- 1] \times (M206 / M238) \times 0.9928\} + \{Uc \times [\exp(\lambda235T) - 1]$
137 $- 1] \times (M207/M235) \times 0.0072\}$

138

139 Where: $_{238}U/(_{235}U+_{238}U) = 0.9928$ and $_{235}U/(_{235}U+_{238}U) = 0.0072$. Uc (U corrected),
140 Th and Pb are concentrations in ppm; T is the age in Ma; M206, M207, M208,
141 M235, M238, M232 are the atomic masses of $_{206}Pb$, $_{207}Pb$, $_{208}Pb$, $_{235}U$, $_{238}U$, $_{232}Th$;
142 $\lambda232 = 0.49475 \times 10_{-4}$ Ma_{-1}; $\lambda238 = 1.55125 \times 10_{-4}$ Ma_{-1}; $\lambda235 = 9.8485 \times 10_{-4}$ Ma_{-1}
143 $_1$ (Pommier et al., 2004).

144 Ages and uncertainties were obtained using EPMA Dating software (Pommier et
145 al., 2004) and age averages were processed using Isoplot 3.75 Excel version
146 (Ludwig, 2012, 2003).

147 Beside the U and Pb values, also the other elements were used for unravelling
148 both mineral chemistry and REE-geochemistry and calculate approximate mineral
149 compositions assuming an idealized monazite formula $Ln^{3+}PO_4$ and considering
150 all elements as part of the mineral lattice (i.e. not specifying possible inclusions or
151 exsolutions of other phases). For the formulae calculations, mineralogical
152 standard normalization procedures were applied (Deer et al., 2013; Perkins,
153 2014), i.e. the transformation of the mean oxide wt-% to mole-%, the distribution
154 of the cations to the four anionic O-sites, and the calculation if the cation and anion
155 charges became balanced.

156 LA-ICP-MS dating has been performed by using aleatory points in all crystals of
157 the three sampling sites LOC (4, 5 and 6) including the same crystals analyzed by
158 EPMA. Analyses were carried out on a single quadrupole Agilent 7700 ICP-MS
159 mass spectrometer coupled to a 193-nm excimer laser system ESI (NWR193UC)
160 in the GeOHeLiS analytical platform of the University of Rennes 1 in France. In
161 the present study, the acquisition time of each analytical spot was set to 80
162 seconds (20 seconds background followed by 60 seconds with the laser firing).
163 Spots diameters of 8 μm associated with repetition rates of 3 Hz with a laser
164 fluency of 5 $J.cm^{-2}$ were used. The signal of $^{204}(Pb+Hg)$ ^{206}Pb, ^{207}Pb, ^{208}Pb, ^{232}Th
165 and ^{238}U masses were acquired. The ^{235}U signal is calculated from ^{238}U based on
166 the ratio $^{238}U/^{235}U = 137.818$ (Hiess et al., 2012).

167 Data were corrected for U–Pb and Th–Pb fractionation and for the mass bias by
168 standard bracketing with repeated measurements of the Moacir monazite
169 reference material (Gasquet et al., 2010). Data reduction was carried out with the
170 software package GLITTER® (Van Achterbergh et al., 2001). Repeated analyzes
171 of the Manangoutry monazite reference material (Paquette and Tiepolo, 2007)
172 treated as unknown were used to control the reproducibility and accuracy of the
173 corrections and yield a concordia age of 548 ± 6 Ma (MSWD=0.98; n=11). After
174 data reduction, U-Th-Pb Concordia diagrams were constructed with the IsoplotR
175 software (Vermeesch, 2018). The calculated Concordia ages are quoted with 95%
176 of confidence interval. More information on the analytical protocol in Poujol M, et
177 al., (2017) and supplementary table in Annex. A.

178

3   Geological background

180 The Guainía Department is located at the northwestern part of the Guiana Shield
181 i.e. a portion of the Colombian part of the Amazon Craton, which extends from the
182 Andean Eastern Cordillera foothills to Venezuela and Brazil and is the least
183 populated and studied area of Colombia. Our geological knowledge of this area is
184 largely based on research conducted in Brazil and Venezuela (e.g., Gansser,
185 1954, 1974; Amaral, 1974; Gaudette et al., 1978; Almeida et al., 1981; Gaudette
186 and Olszewski, 1985; Bettencourt et al., 1999; Tassinari et al., 1999 and (Santos
187 et al., 2000), although important studies have been done recently also in Colombia
188 (e.g., Bonilla et al., 2013, 2016, 2019; Cordani et al., 2016, Ibanez et al., 2011,
189 Kroonenberg, 2019).

190 According to Santos (2003), the crystalline basement in the Western Guiana
191 Shield is linked to the Rio Negro geochronological province 1.82 – 1.52 Ga (Figure
192 1).

193
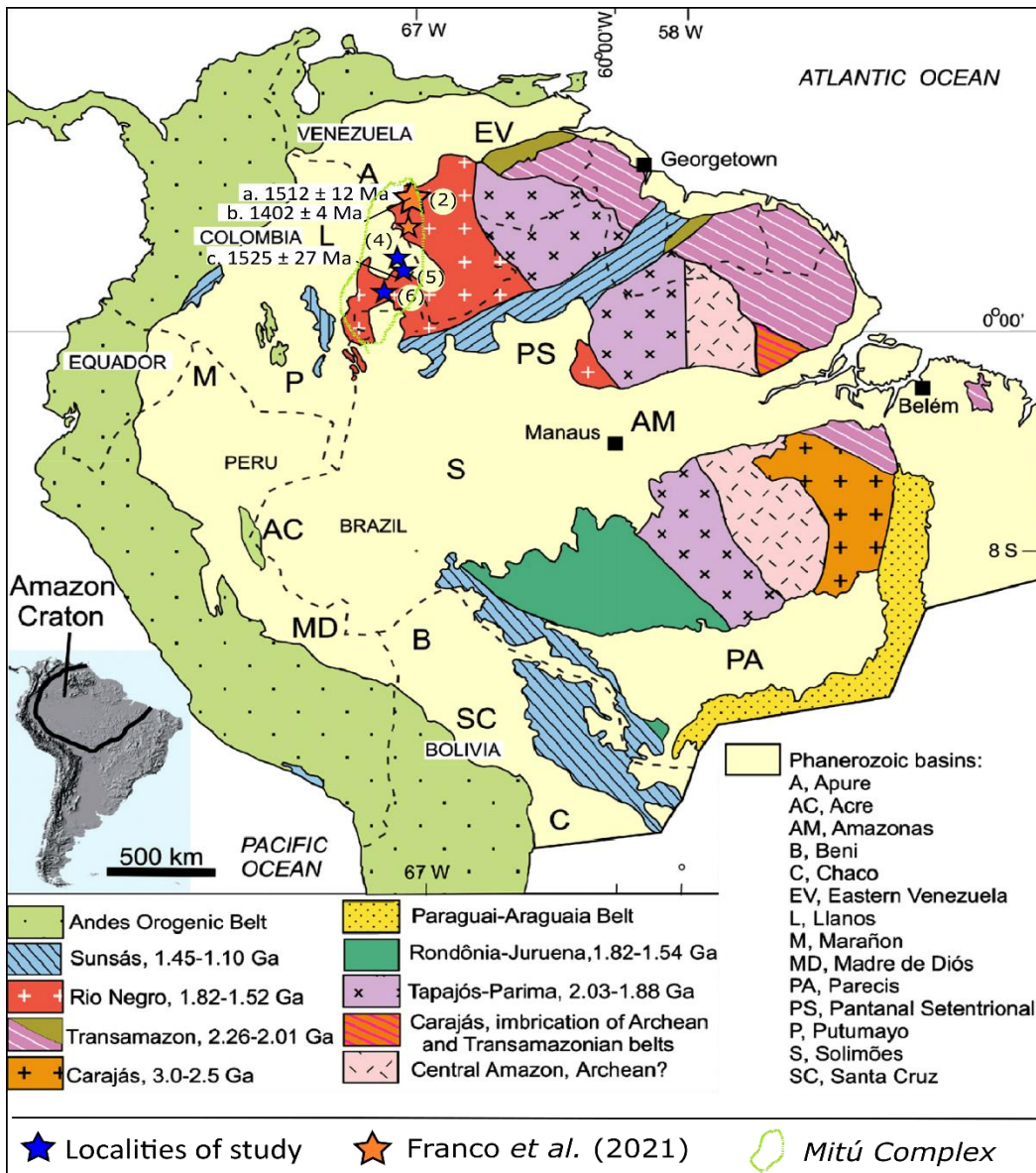
Figure 1. Regional map showing the geochronological provinces and some ages in Ma reported for rocks and minerals in and outside the study area: a. U-Pb in rutile (Nb,Ta) from Cachicamo hills; b. U-Pb in zircon from the basement zone (Bonilla et al., 2013); c. U/Pb in zircon from granitic rocks of Tabaquen in the Guainía River Bonilla (2019). Modified from Santos et al. (2008).

Enhanced by the PRORADAM program (Galvis Vergara et al., 1979a; Huguett et al., 1979) the complex geological history of Colombia since the Proterozoic has been slowly revealed, with different phases of extension and compression, orogenesis, erosion, sedimentation, metamorphism and emplacement of a wide variety of magmatic rocks. Hallmarks in descriptions represent Celada et al. (2006) and recently Kroonenberg (2019) synthetized the actual geological information of E-Colombia.

207 Different orogenic episodes in the Guiana Shield have been recognized so far
208 (Kroonenberg 2019): the Transamazonian Orogeny (2.26 to 1.98 Ga) in the
209 Eastern margin (as result of the collision with Proto-Africa); the Querarí Orogeny
210 (1.86–1.72 Ga) at the Western border between Colombia, W-Venezuela and NW-
211 Brazil; and, in the framework of the Rodinia supercontinent formation, the
212 Grenvillian Orogeny (1.3–1.0 Ga), called Putumayo Orogeny by Ibáñez-Mejía et
213 al. (2011) as revealed by some inliers in the Andes but also eastward by gabbroic
214 intrusions (Bonilla Perez et al., 2020).

215 In the Guainía Department between the Guaviare River to the north, the Caquetá
216 River to the south, and the Chiribiquete mountain range to the west only very few
217 outcrops have been studied in the past. The oldest rocks seem to be felsic to
218 intermediate metavolcanic rocks along the Atabapo River and parts of the Río
219 Negro River, which Galvis et al. (1979) and Huguett et al. (1979) named "Neises
220 del Atabapo-Río Negro" (see López et al., 2010). Kroonenberg (2019) proposed
221 that they do not belong to the Mitú-Complex but rather to the Mid-
222 Paleoproterozoic Caicara Metavolcanics and associated them with the 1984 ± 9
223 Ma Surumu Rhyodacite (SHRIMP U-Pb in zircons, Santos et al., 2003).

224 The Colombian basement was first described as the "Basement Group" (Gansser,
225 1954) or as the "Guyanese Complex" (Pinheiro et al., 1976), then as the Migmatitic
226 Mitú Complex (Galvis Vergara et al., 1979b) and later as the Mitú Complex (López
227 Isaza, 2012; López Isaza et al., 2007; López Isaza and Cramer, 2012). Its
228 extension has been initially inferred based on geophysical data. Most of this
229 basement is constituted by Precambrian crystalline rocks. It is covered by
230 Cenozoic sediments, as well as by a thick tropical forest covering peneplanes
231 modeled by strong tropical weathering and meandering rivers in extensive alluvial
232 plains, locally interrupted by inselbergs of the old basement.

233 The Mitú Complex is composed of high-grade metamorphic rocks and granitoids
234 with various compositions and affinities, formed during different orogenic events
235 (Kroonenberg, 2019; López Isaza et al., 2007). The metamorphosed igneous and
236 sedimentary protoliths appear mainly as quartz feldspathic gneisses with alaskite
237 to monzonite composition, but also as amphibolite, quartzite, metagranitoids,
238 calco-silicate (rich in epidote group minerals) and quartz gneisses, some of them
239 with migmatitic structures.

240 Large parts of the Mitú Complex (Figure 2) are composed of monzogranites with
241 calc-alkaline affinities, besides meta- to peraluminous granites (U-Pb in zircon LA-
242 MC-ICP-MS Concordia age of 1574 ± 10 Ma for the Mitú granite; Ibáñez-Mejía et
243 al., 2011), as well as of other granites. Among the clearly metamorphic rocks,
244 quartz-feldspathic gneisses are the most abundant with U-Pb zircon ages
245 between 1800-1760 Ma (Bonilla et al., 2019; Cordani et al., 2016; Kroonenberg,
246 2019; López et al., 2007). Medium grade amphibolite facies metamorphic rocks
247 within a series of essentially juvenile magmatic arcs in the Rio Negro Juruena
248 province are interpreted by several workers as subduction-related (Cordani et al.,
249 2016; Tassinari and Macambira, 1999).

250 Younger granitoids in the southeastern part (especially Guainía Department)
251 exhibit variable compositions, porphyritic textures and may contain feldspar
252 phenocrysts. They were emplaced ca. 1750 Ma ago during the Statherian (Bonilla
253 et al., 2019) while some two-mica granite intrusions are 1600-1550 Ma old (Bonilla
254 et al., 2019). It must be noticed that other ~1600 – 1500 Ma old granites have
255 been described along the whole Colombian eastern territory (Cordani et al., 2016;
256 Ibañez, 2010; Priem et al., 1982; Rodriguez et al., 2011).

257 The Parguaza batholith, emplaced 1550-1500 Ma ago, represents a primary
258 source of Sn, Nb, Ta and REE mineralization (Aarden and Davidson, 1977;
259 Herrera-Bangerter, 1989; Mariño, 2012; 2013) although it is largely covered by
260 partially lateritic Cenozoic sediments in plains and valleys. In the Venezuelan
261 localities of El Burro, La Fortuna and Aguamena, colluvial - alluvial deposits
262 contain sub-to economic concentrations of minerals such as cassiterite, rutile-
263 (Nb,Ta), columbite-tantalite and REE minerals.

264 An important feeder of rare element minerals in the Parguaza Batholith seem to
265 be pegmatites, and similarly pegmatites associated to the Mitú Complex (e.g.
266 López Isaza and Cramer, 2012) may also be the main primary source of the
267 monazites and xenotimes discussed here.

268 **4   Pegmatites**

269 Due to their economic importance and variability, manifold pegmatite classification
270 efforts (e.g. Ginsburg et al., 1979) were developed over time which are still
271 controversial and object of research. Thus Černý (1991) proposed the existence
272 of two main pegmatite families, the LCT (Li-Cs-Ta) and the NYF (Nb-Y-F), a
273 concept however only applicable for highly fractionated pegmatites if exotic
274 minerals such as spodumene, tantalite, pyrochlore, pollucite, etc. are present
275 (London, 2018). Černý and Ercit (2005) and Černý et al. (2012) defined, based on
276 metamorphic environment, mineralogy, elemental composition and texture, five
277 pegmatite classes from which four may host Ta–Nb–Sn mineralization (especially
278 the abyssal, muscovite-rare-element, rare-element and miarolitic classes) and 10
279 subclasses. The rare-element class is the most important for Nb–Ta
280 mineralization, which are further subdivided depending on major and minor
281 minerals carrying Li, Be, REE and Nb–Ta.

282 Most of the pegmatites with the LCT signature have compositional affinity with S-
283 type granites (Chappell and White, 1974, 2001). Their protoliths are assumed to
284 be pelitic marine sediments as source of Al - and trace elements enrichment like
285 B, Be, P and Sn. From those after anatectic melting of metamorphic schists and
286 gneisses, reduced granites and derived specialized pegmatites could form with
287 high contents in Li, Cs, Ta where fluxing components like B, P, and F play an
288 important role. Many of these trace elements with different grades of
289 incompatibility are contained in micas and feldspars and liberated during the melt-
290 forming reactions and may concentrate furthermore in specialized pegmatites
291 above the mineralization limit, i.e. forming abundant and large visible minerals

292 characteristic of many famous and economic important pegmatite ore deposits
293 worldwide.

294 On the other hand, most of the NYF-family pegmatites are thought to be derived
295 from A-type granites, where "A" may mean "anorogenic" (e.g. Eby, 1990) but also
296 Al-rich or abnormal and their origins are debatable. For example, Frost and Frost
297 (2014) emphasized their higher Fe-content and proposed to name them ferroan
298 alkali-calcic to calc-alkalic granitic rocks. Their source may be gneissic granulites
299 deep in the continental crust, with some mafic mantle contribution or low-density
300 carbonic fluid. The NYF-family contains chemically complex oxides and silicates
301 that carry heavy rare earth elements (HREE), Ti, U, Th, and Nb > Ta (Cerný et al.,
302 2012). Abundant fluorite or topaz reflects the enrichment in fluorine. The NYF
303 pegmatites are depleted in phosphorus, and tourmaline is uncommon.

304 Subduction-related I-type granites may be a smaller source both of LCT and NYF
305 pegmatites (Černý and Ercit, 2005), but there are a lot of pegmatites worldwide,
306 which may or may not fit clearly in any of these models (Bonin, 2007; Cerný et al.,
307 2012; Dall'Agnol et al., 1999; Dill, 2015; Dill et al., 2006; Gandhi and Sarkar, 2016;
308 Kroonenberg et al., 2016; Laznicka, 2006; London and Morgan, 2012; Sial et al.,
309 2011).

310

311 **5   Selected mineral occurrences**

312 The Guainía region is mostly covered by humid tropical forests and extensive
313 alluvial plains with preferably west-east drainage of the main rivers Guaviare,
314 Inírida, Guainía and Cuyarí to the Orinoco and Amazonas rivers, which constitute
315 also the main ways of communication between local indigenous communities and
316 non-local population. During several fieldtrips, sediments and basement rocks
317 outcropping along the main rivers including inselbergs like Mavicure, Espina,
318 Tortuga, Tabaquen, Matraca and Danta were sampled, and from Vichada to
319 Guainía departments, four localities from north to south were defined for more
320 detailed studies and are described elsewhere, especially the Cachicamo rutiles-
321 (Nb), closely associated to the Parguaza Batholith (Franco et al., 2021). For this
322 study, we analyzed three of them in the Guainía Department (Figure 2): LOC (4)
323 near to the Inírida River and the Espina hills, LOC (5) near to San Jose at the
324 Guainía River, and LOC (6) near to Barranquilla at the Cuyari River.
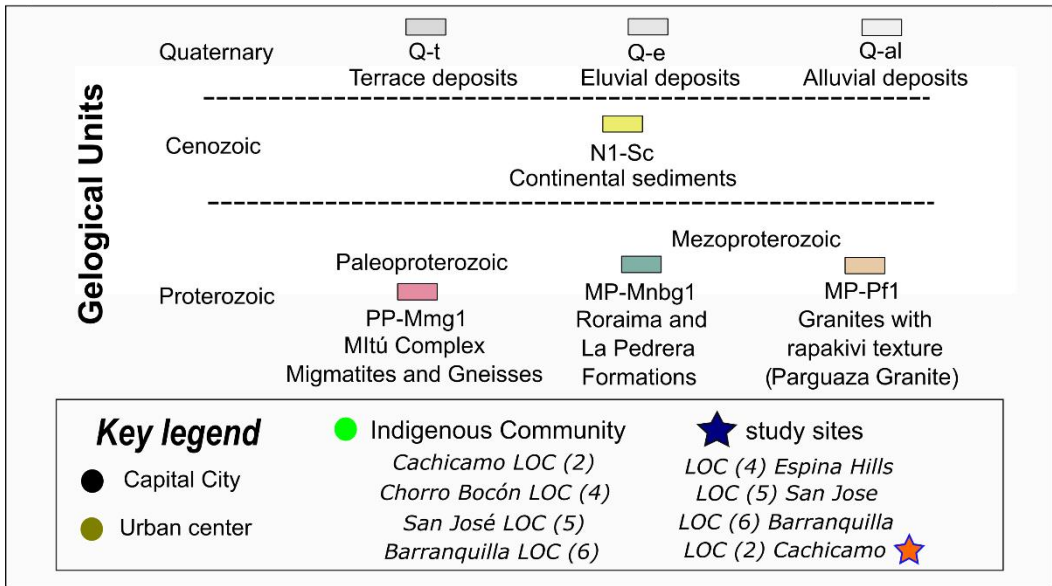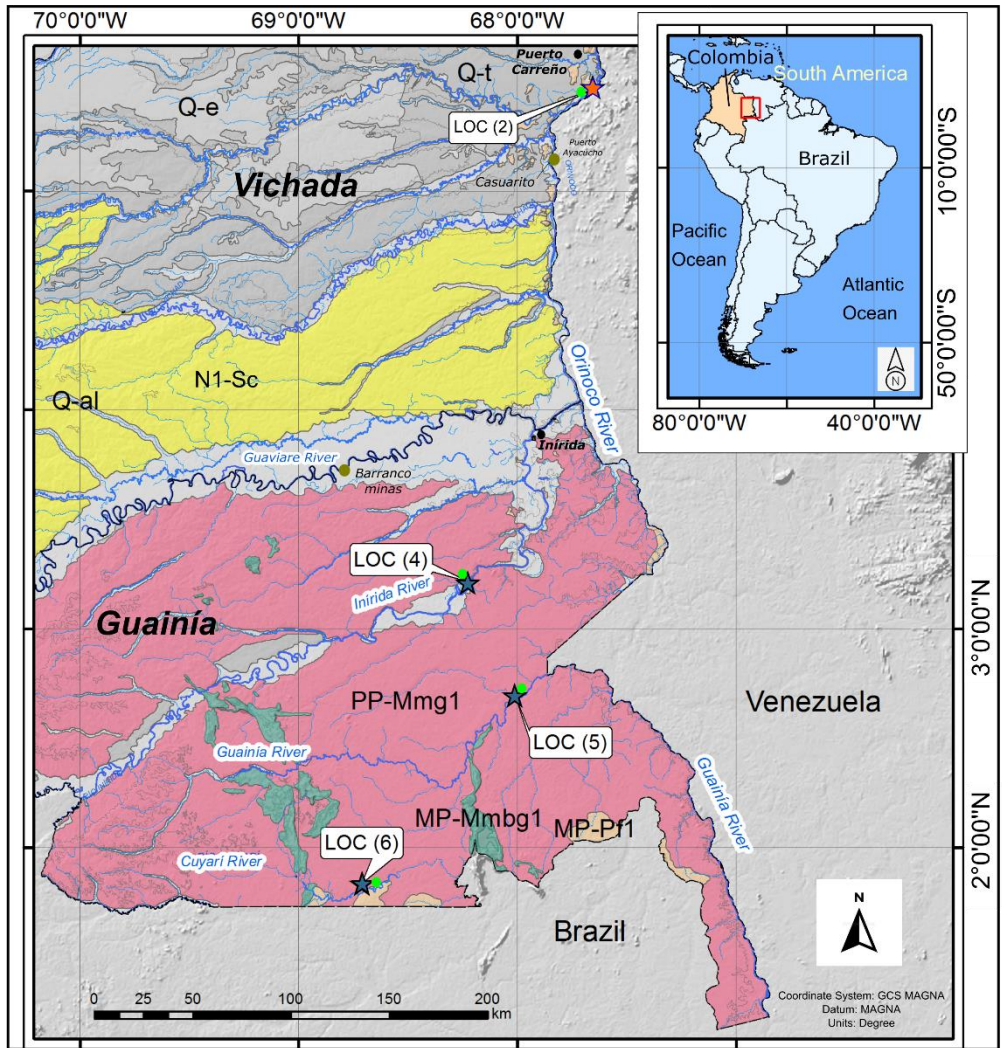
Figure 2. Generalized geological map of Vichada and Guainía Department, eastern part of Colombia showing the localities (4, 5 and 6) (blue stars) and locality (2) (pink star) -

328　from which localities (4 to 6) were selected for this study; locality (2) associated to the
329　Parguaza Granite was studied by Franco et al., (2021) and is here shown for a better
330　overview. As green dots the names of the communities nearby the sampling locations.
331　Modified from the Geological Map of Colombia (Gómez Tapias et al., 2015).

332

5.1　Monazite, xenotime and Nb, Ta, U, Zr-minerals from Espina hills - Inírida River LOC (4)

335　In the Espina foothills as main mineralization site of LOC (4) N 03° 12' 13.6'', W
336　068° 09' 19.6'' (Figure 2), monazite occurs in colluvial deposits with large blocks
337　of quartz and muscovite pegmatites. Monazite crystals can reach up to 1 cm in
338　length and are associated with rutile-(Nb,Ta), xenotime, REE-enriched zircon and
339　U-Th bearing minerals and, in some cases, black tourmalines in the panning
340　concentrates (Figure 3).
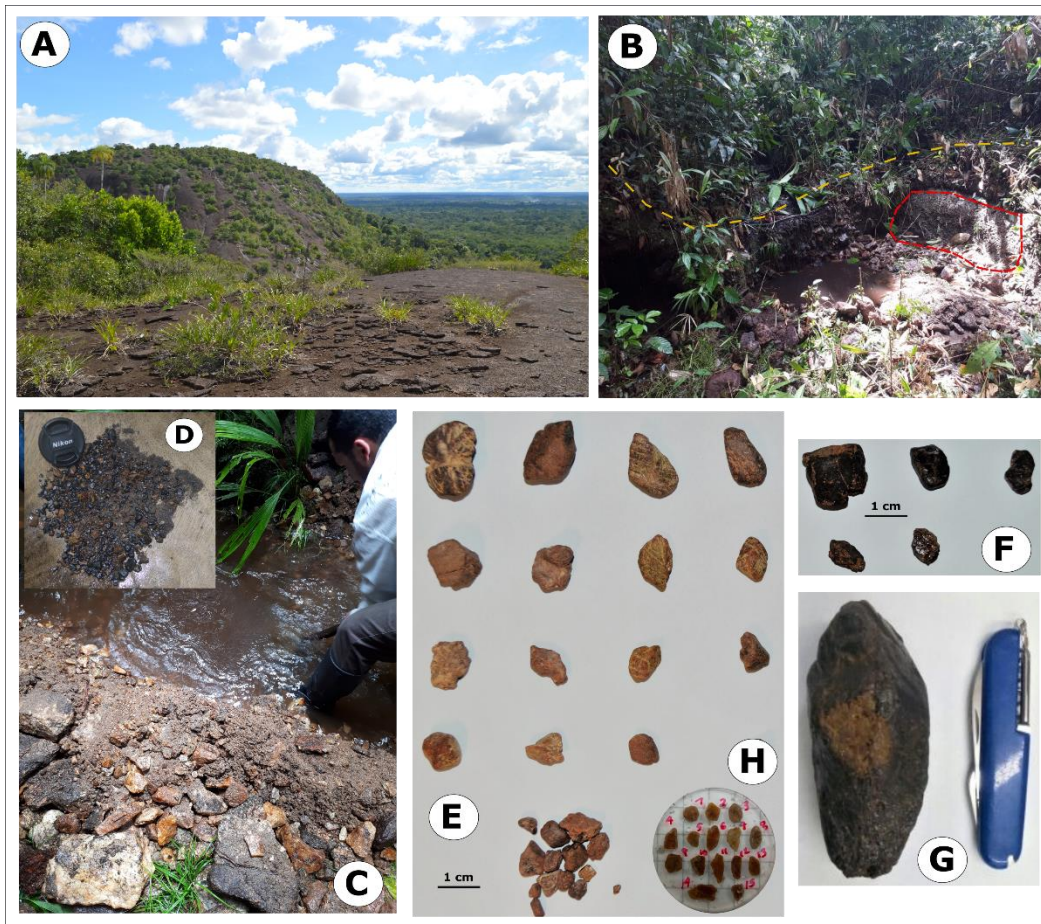
341

342　Figure 3. Pictures of field and mineral found in panning concentrates from LOC (4) Espina
343　Hills. A. view from the top of Espina Hills; B. colluvial deposits in the foothill of Espina Hills
344　(yellow line shows the limit of the dissectect colluvium and red line basement rock); C and
345　D. sample site and heavy mineral concentrate and pan concentrate, respectively; E.
346　Monazite and xenotime crystals selected from the pan concentrates; F. U-Th bearing
347　minerals; G. Rutile-(Nb) associated to monazite (brown color) and H. Polished epoxy resin
348　puck of monazite for analysis.

5.2 Monazite and Ta, Nb-minerals at the San Jose - Guainía River LOC (5)

Near to the Indigenous community of San José labelled LOC (5) N 02° 41' 59.6'', W 068° 01' 38.4'' (Figure 2), monazite grains were found in the regoliths overlying pegmatitic dykes emplaced in gneiss and migmatites of the Mitú Complex. However, the most representative crystals occur in colluvium deposits together within blocks and gravels of quartz and muscovite dyke fragments along the Seje and Lombriz creeks. Monazite crystal can reach up to 3 cm in length and are found together with Fe-columbite, rutile-(Nb,Ta) and magnetite (Figure 4). Occasionally isolated xenotime and tourmaline crystals are found in the panning concentrates.

Figure 4. Pictures of field and mineral found in panning concentrates from LOC (5) San Jose. A. view of rocks of Mitú complex in the Guainía River at San Jose indigenous community; B. Pegmatite with an elevated radioactivity measures; C. Pegmatite with Fe-columbite crystal; D. Sample site of heavy mineral concentration E. Fe-columbite crystals from pan concentrates; F; Huge monazite crystals from pan concentrates; G. Monazite crystals selected from the pan concentrates and H. Polished epoxy resin puck of monazite for analysis.

5.3 Monazite and Ta, Nb, Zr and REE-minerals from Barranquilla - Cuyari River LOC (6)

Monazite grains were found near Barranquilla labelled LOC (6) N 01° 48' 51.9'', W 068° 41' 12.5'' (Figure 2), in colluvium deposits cut by small drains along the

371 Cuyari River basin, together with smoky quartz blocks, muscovite, beryl and Fe-
372 columbite dikes as well as K-feldspar, quartz and garnet bearing dikes. They are
373 related to plutonic rocks from syeno-granites to acidic granites, some of them with
374 rapakivi texture. Monazite can reach up to 0,5 cm in length and are found together
375 with Fe-columbite, Mn-Tantalite, rutile-(Nb,Ta), xenotime, zircon, and garnet
376 (spessartine) (Figure 5). Isolated crystals of black tourmaline occasionally occur
377 in panning concentrates.
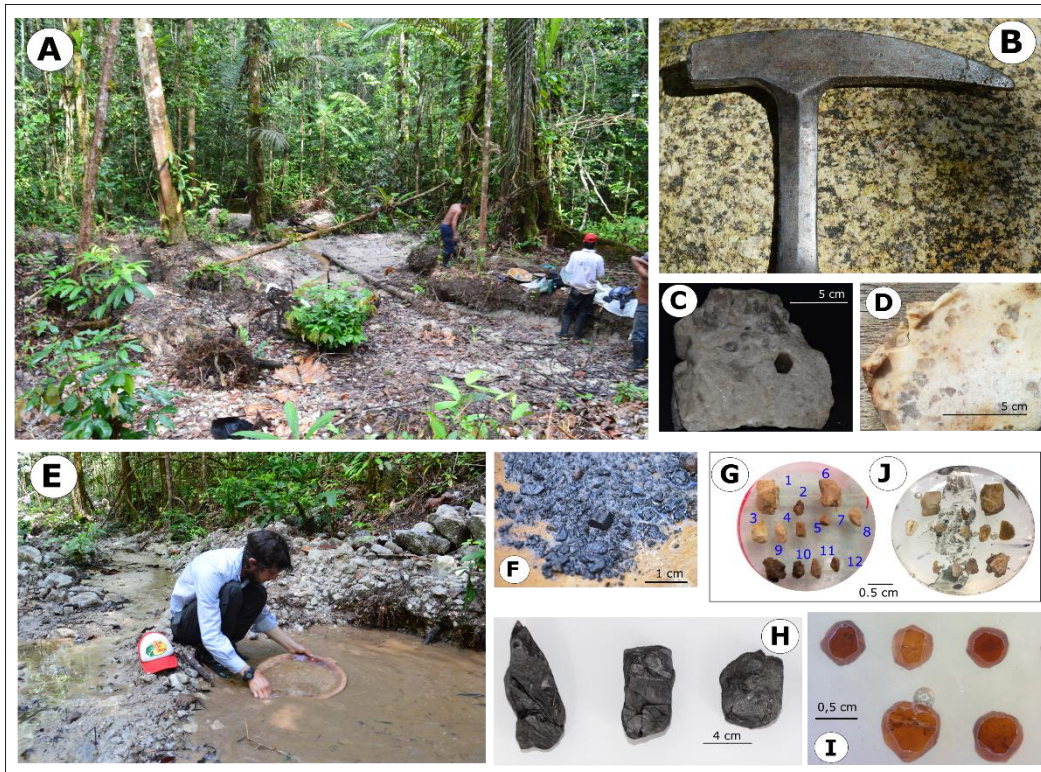
378

379 Figure 5. Pictures of field and mineral found in panning concentrates from LOC (6)
380 Barranquilla. A. Colluvial deposits explored by local people from Barranquilla indigenous
381 community; B. Block of two mica granite founded in the base of colluviums; C. Pegmatite
382 with a retaining the shape of a beryl crystal y D Sample of K-feldspar - garnet pegmatite;
383 E. Sample site of heavy mineral; F. Heavy mineral concentrate; G. Monazite crystals
384 selected from the pan concentrates (1-5); H. Columbite-tantalite crystals; I. Garnet crystals
385 and J. Polished epoxy resin puck of monazite for analysis.

386 **6   Results**

387 **6.1   Monazite chemistry**

388 The pXFR-measurements were in good qualitative agreement with the EPMA data
389 (supplementary Table in Annex A) which reveal that all the monazite crystals are
390 Ce and La dominated. As the BSE-images Figure 7 show very inclusion-poor
391 monazites, the calculated mineral formulae should be very near to the real
392 monazite compositions. The HREE Ho, Er, Tm, Yb and Lu were below EPMA-
393 detection limit. In LOC (4), monazite grains are very homogeneous with Ce_2O_3
394 between 29 and 31% and ThO_2 between 8 and 9 %. The standard deviation

395   among the 7 measured monazite crystals of the main cations is below 0,1%. Their
396   average formula including all elements could be expressed as
397    $Ce_{0.44}La_{0.16}Nd_{0.16}Sm_{0.04}Y_{0.03}Gd_{0.02}Dy_{0.01}Pr_{0.05}Th_{0.08}Pb_{0.01}Ca_{0.05}Si_{0.05}P_{0.91}O_{3.94}$.

398   Monazite crystals from LOC (5) show a more heterogeneous composition with
399   Ce_2O_3 between 27 and 34% and ThO_2 between 4 and 13 % resulting in standard
400   deviations (n=8) of 7% for Th, and around 1% for La, Ce, Sm and Ca.

401   Their average formula would be $Ce_{0.44}La_{0.16}Nd_{0.14}Pr_{0.04}Sm_{0.04}Y_{0.03}Gd_{0.02}$
402    $Dy_{0.01}Th_{0.09}Ca_{0.07}Pb_{0.01}Si_{0.05}P_{,0.91}O_{3.94}$.

403

404   In LOC (6), monazite grains are still less heterogeneous than in LOC (4) and LOC
405   5 with Ce_2O_3 between 26 and 29% and ThO_2 between 9 and 12 %. The REE
406   standard deviations (n=10) are around or below 0,1%. Their average formula
407   would be:

408    $Ce_{0.42}La_{0.13}Nd_{0.19}Pr_{0.05}Sm_{0.05}Y_{0.05}Gd_{0.02}Dy_{0.01}Th_{0.10}Ca_{0.04}Pb_{0.01}Si_{0.08}P_{0.86}O_{3,94}$.

409

410   In all 3 sites, the sum of cations including P is 2, assuming an idealized monazite
411   formula $LnPO_4$. Phosphor and oxygen deficits in all the formulas of the three sites
412   are probably due to cation charge balance vacancies, especially of $Ce^{(3+, 4+)}$, and
413   possible occupancy of elements like Si on the P-site.

414

415   Also, the chondrite-normalized REE distribution patterns in Figure 6 for the
416   monazite crystals from LOC (4, 5 and 6) are very similar among each another.
417   Their REE pattern is much closer to granitic than pegmatitic monazites as defined
418   by Zhu and O´Nions (1999), especially exhibiting higher La and Ce contents than
419   the pegmatitic reference monazites. The Gd and Dy depletion is characteristic of
420   the monazite structure, and HREE enter preferentially in minerals like xenotime,
421   as garnet is nearly absent.

422

423
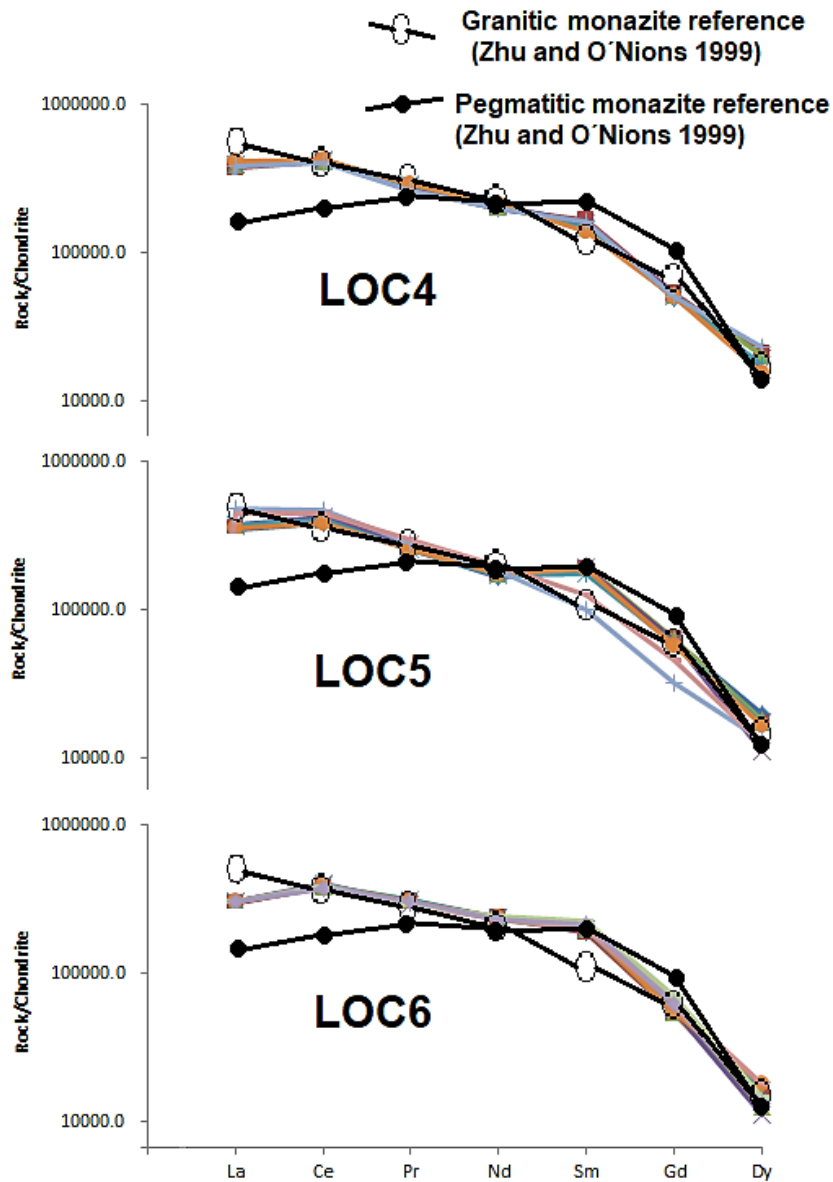
Figure 6 Chondrite-normalized (Sun and McDonough, 1989) REE patterns of the investigated monazites (Ho, Er, Tm, Yb and Lu below EPMA-detection limit) and comparison with pegmatitic and granitic monazites after Zhu and O´Nions (1999). Observe the higher coincidence of E-Colombian monazites with those of granitc origin with higher La and Ce in comparision to Zhu and O´Nions (1999) pegmatitic monazites.

6.2 Geochronology

6.2.1 EPMA U-Th-Pb chemical ages

Th and Pb contents of all dated monazite grains are relatively high which helps to minimize background related errors (Jercinovic et al., 2008). Seven analyses of the monazite crystal from LOC (4) in Espina Hills yield an EPMA age of 1390 ± 17 Ma (2σ, MSWD = 0.59) (Figure 7A). Eight analyses from the San Jose monazite crystal LOC (5) return a chemical age of 1523 ± 20 Ma (2σ, MSWD = 1.3) (Figure 7B). Ten spots on a single monazite grain from Barranquilla LOC (6) yield a chemical age of 1527 ± 13 Ma (2σ, MSWD = 0.27) (Figure 7C).
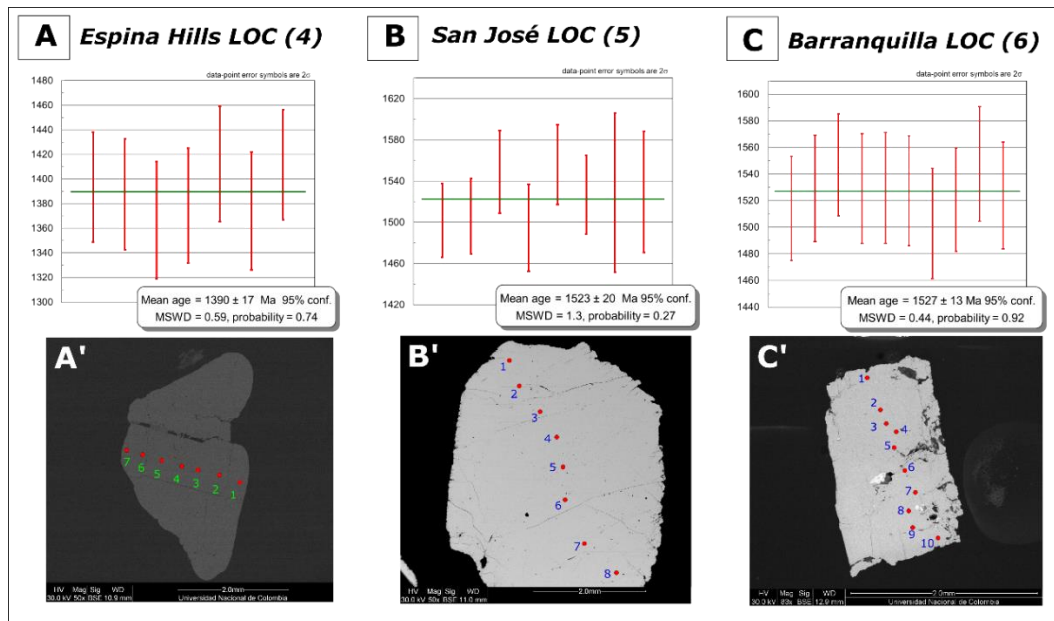
Figure 7. EPMA U-Th-Pb average ages calculated for each sample corresponding to Espina Hills (A), San José (B) and Barranquilla (C) localities. Data point errors are reported as 2σ. Below, BSE images of the corresponding monazite crystals showing the analyzed points (A', B' and C'). Data table in Annex B.

6.2.2 LA-ICP-MS U-Th-Pb ages

The twenty-two analyses in 15 monazite grains from LOC (4) expressed as $^{208}Pb/^{232}Th$ versus $^{206}Pb/^{238}U$ concordia diagram (Figure 8A) plot all in a concordant position and yield a concordia age of 1346 ± 18 Ma (MSWD (conc+equiv) = 1).

The fourteen analyses in 10 monazite grains of sample LOC (5) plot all in a concordant position (Figure 8B). Although they spread along the concordia curve with apparent ages from 1606 down to 1468 Ma, they yield a relatively well constrained concordia age of 1525 ± 15 Ma (MSWD (conc+equiv) = 1.9).

The fourteen analyses in 5 monazite grains of sample LOC (6) plot in a concordant position (Figure 8C). Two analyses (grey lines in Figure 8C) yield apparent ages of 1605 and 1650 Ma, respectively. However, the twelve remaining analyses yield a well-constrained concordia age of 1522 ± 16 Ma (MSWD (conc+equiv) = 1).
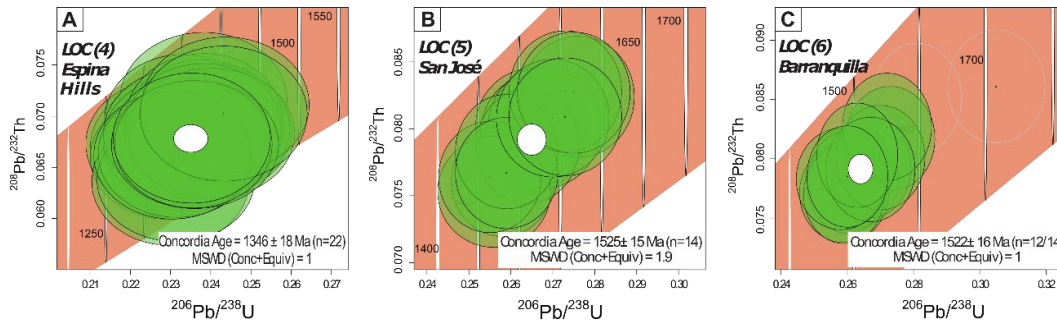
Figure 8. LA-ICP-MS monazite concordia ages of localities 4-6: Espina Hills (A), San José (B) and Barranquilla (C). Data table in Annex C. Data errors are reported at 2σ.

7 Discussion

7.1 Chemical data

The samples from this study were collected at the surface from colluvial deposits, weathered zones, and rock fragments, without the possibility of studying the magmatic to pegmatitic bodies present at depth. However, the geological, mineralogical, and geochemical data allow us to draw some preliminary, although contradictory conclusions about the three sites.

The chemical data suggest that the monazite crystals from all sites are very similar despite their distance of 70-150 km among each another. They are consistent with a granitic to pegmatitic origin, but without reaching highly specialized rare elements pegmatite characteristics. Parts of the mineral assemblage are indicative of a NYF-family affinity, with a geochemical signature Nb>Ta, Ti, Y, Sc, REE, Zr, U, Th, F (Černý and Ercit, 2005).

Melcher et al. (2017) proposed a possible NYF-family affinity for placer tapiolite, ixiolite, CGM (columbite group minerals) and rutile samples from not specified E-Colombian sites. One of their columbite, rutile and ixiolite samples however was collected near Barranco Minas at the Guaviare River (Figure 2). The presence of cassiterites and some personal information from the authors demonstrate that most of these samples were collected within the Vichada Department associated with the Parguaza Rapakivi Granite intrusion (see LOC (2) in Figure 2), which is also in agreement with the higher Sn-contents reported by Melcher et al., (2017). However, cassiterites were not found in panning concentrates in the Guainía Department study area. In the ixiolite and CGM-samples those authors also observed a CI-chondrite normalized HREE-enrichment trend and negative Eu and Y anomalies (Melcher et al., (2017).

Chappell and White (2001) recognized based on whole rock geochemistry an elevated phosphorus content as diagnostic of the S-type granites, and hence of LCT-pegmatites, whereas the NYF pegmatites are depleted in phosphorus,

492   tourmaline is uncommon and abundant fluorite or topaz would reflect the
493   enrichment in fluorine (Cerný et al., 2012). If this is true, the abundant monazite,
494   xenotime, and black tourmaline concentrations in the three sampling sites as well
495   as the absence of fluor-bearing minerals advocate against a NYF affinity. The
496   REE-monazite data of Zhu and O´Nions (1999) suggest a more granitic than
497   pegmatitic origin of the mineralizations but are only one indication. Also, as the
498   samples are from colluvial deposits, it may be that the two families of pegmatites
499   (LCT and NYF) have been eroded and contributed to the overall chemical and
500   mineralogical composition of the studied samples. We can therefore at this stage
501   conclude that the mineralogical and geochemical data are not very conclusive to
502   propose a clear affinity but support a more complex genesis that involve different
503   primary sources related with S- and A-type granites from which mineralized
504   pegmatites may have evolved.

505

7.2   Age and interpretations

507   We used EPMA and LA-ICP-MS as complementary technique, EPMA in this study
508   was use for acquiring the chemical composition of the monazite as well as for
509   calculating the chemical age while LA-ICP-MS was used to measure the isotopes
510   U-Th-Pb for calculating directly the ages in a faster way which is better to do
511   provenance analysis. LOC (5 and 6) yield an EPMA chemical and LA-ICP-MS
512   ages of 1523 ± 20 Ma and 1525 ± 15 Ma and 1527 ± 13 Ma and 1522 ± 16 Ma
513   respectively, all within the error, however LOC (4) yield an EPMA chemical and
514   LA-ICP-MS ages of 1390 ± 17 Ma and 1346 ± 18 Ma respectively, a difference of
515   ~45 Ma was found. This difference may be attributed to EPMA measurements due
516   to imperfections in polishing. BSE Images (Figure 9) revealed a homogeneous
517   non-zoned without inclusion monazite crystals for the three localities. For the other
518   hand xenotime from the same pan concentrate used for LOC (4) yield an LA-ICP-
519   MS U-Pb age of 1390 ± 8 Ma (unpublished data yet) that coud be related.

520
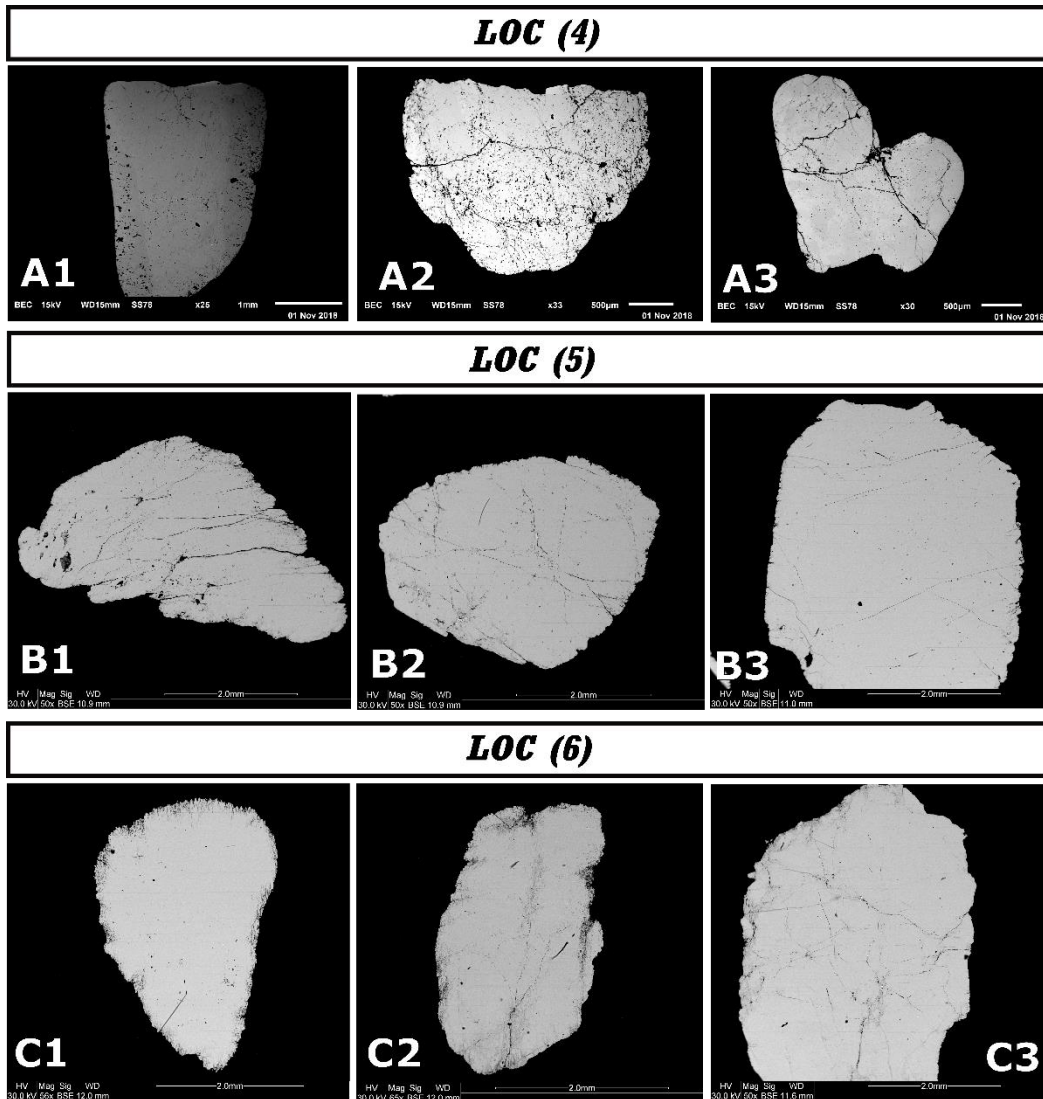
Figure 9. BSE images for some crystals use for LA-ICP-MS dating for the three localities showing a very homogeneous crystals of monazite. showing a rich thorium mineral were observed; (A1, 2 and 3) Monazite crystals from LOC (4); (B1, 2 and 3) Monazite crystals from LOC (5), small inclusion < 30 µm of Th mineral was observed; (C1, 2 and 3) Monazite crystals from LOC (6).

7.2.1 Age relation with the surrounding rocks

The oldest EPMA and LA-ICP-MS based ages at LOC (4) 1390 ± 17 Ma and 1346 ± 18 Ma, LOC (5) 1523 ± 20 Ma and 1525 ± 15 and LOC (6) 1523 ± 20 Ma and 1525 ± 15 Ma, respectively, indicate a crystallization age similar to Mesoproterozoic anorogenic intrusions recorded in homogeneous anorogenic A-type granites present in the study area (Table 1). This magmatic episodes represented by anorogenic granites in the surroundings of the Orinoco, Guainía, Inírida and Cuyari Rivers may be locally related with coeval granites from Vaupés River and regionally with rapakivi granites of the Pijiguaos range and Parguaza in

536 Venezuela with reported ages of 1545-1500 Ma and in Brazil with granites from
537 the intrusive suite of Serra da Provincia with U-Pb ages of 1600-1532 Ma (see
538 Table 1), intruded at the end of the Rio Negro Juruena orogeny. Several of these
539 intrusive rocks and their post magmatic phases are the primary source of Sn, Ta,
540 Nb and Ti mineralizations.

541 The crystallization ages obtained from the monazite crystals from the three
542 localities are comparable with those from exposed Mesoproterozoic rocks such
543 as Parguaza in Venezuela and Vichada, Colombia from Orinoco River, Danta and
544 Matraca granites from the Inírida River, Tabaquen and similar granites from the
545 Guainía River and the rapakivi granites from the Cuyarí River reported in the
546 Guainía Department (see Figure 2 and Table 1)). The oldest obtained age range
547 of 1527-1525 Ma from the localities (5, 6) may correspond to monazite
548 mineralization from pegmatitic rocks related to granites near to Tabaquen and San
549 José with U-Pb ages of 1606-1525 Ma and rapakivi granites at Cuyarí River with
550 ages between 1550 -1600 Ma, and the younger ones in the locality (4) with an
551 age range of 1346 to 1390 Ma could correspond to monazite mineralization from
552 pegmatites of Espina, Danta and Matraca granitic rocks, the last one with an age
553 of ~1343 Ma (Table 1).

554

555 Table 1. Compiled ages of some Mesoproterozoic granites from Colombia, Venezuela,
556 and Brazil including the isotopic method use to dating

Locality	Country	Isotopic system	Age (Ma)	Reference
Murciélago Hill (Rapakivi granite)	Colombia	Ar/Ar	1237 ± 13	SGC (2013)
Murciélago Hill (Rapakivi granite)	Colombia	Ar/Ar	1292 ± 8	SGC (2013)
Angelita Hill (Rapakivi granite)	Colombia	Ar/Ar	1359 ± 8	SGC (2013)
Bita Hill (Rapakivi granite)	Colombia	Ar/Ar	1361 ± 9	SGC (2013)
La Hormiga Hill (Rapakivi granite)	Colombia	Ar/Ar	1359 ± 8	SGC (2013)
La Hormiga Hill (Rapakivi granite)	Colombia	Ar/Ar	1339 ± 8	SGC (2013)
La Hormiga Hill (Rapakivi granite)	Colombia	Ar/Ar	1366 ± 9	SGC (2013)
La Hormiga Hill (Rapakivi granite)	Colombia	Ar/Ar	1366 ± 9	SGC (2013)
La Hormiga Hill (Rapakivi granite)	Colombia	Ar/Ar	1376 ± 14	SGC (2013)
La Hormiga Hill (Rapakivi granite)	Colombia	Ar/Ar	1383 ± 8	SGC (2013)
La Venturosa (Rapakivi granite)	Colombia	Ar/Ar	1368 ± 14	SGC (2013)
La Venturosa (Rapakivi granite)	Colombia	Ar/Ar	1361 ± 8	SGC (2013)
Tomo River (Rapakivi granite)	Colombia	U/Pb	1392 ± 5	Bonilla et al. (2013)
Cachicamo Hills (Rapakivi granite)	Colombia	U/Pb	1402 ± 2	Bonilla et al. (2013)
Inírida River, Matraca and Danta rapakivi granites	Colombia	U/Pb	1343 ± 8	Bonilla et al. (2016)

Locality	Country	Isotopic system	Age (Ma)	Reference
Apaporis River (Syenogranite)	Colombia	U/Pb	1593 ± 06	Ibañez-Mejia et al. (2011)
Apaporis River (Syenogranite)	Colombia	U/Pb	1578 ± 27	Ibañez-Mejia et al. (2011)
Apaporis River (Monzogranite)	Colombia	U/Pb	1530 ± 21	Ibañez-Mejia et al. (2011)
Vaupés River (monzogranite)	Colombia	U/Pb	1574 ± 10	Ibañez-Mejia et al. (2011)
Mitú granite	Colombia	U/Pb	1552 ± 34	Priem et al. (1982)
Raudal Morroco Inírida River (Monzogranite)	Colombia	U/Pb	1507 ± 22	Cordani et al. (2016)
Mitú range (Monzogranite)	Colombia	U/Pb	1510 ± 26	Cordani et al. (2016)
Matraca granite - Inírida River	Colombia	U/Pb	1343 ± 8	Bonilla et al. (2016)
Granites of the Guainía River	Colombia	U/Pb	1606 ± 46	Bonilla et al. (2019)
Granites of the Guainía River	Colombia	U/Pb	1525 ± 27	Bonilla et al. (2019)
Cuyari River (Porphyritic granite)	Colombia	U/Pb	1596 ± 52	Bonilla et al. (2019)
Marieta River, Marieta Granite	Venezuela	Rb/Sr	1340 ± 10	Cited in Barrios et al. (1985)
San Pedro Granite	Venezuela	Rb/Sr	1372 ± 10	Cited in Barrios et al. (1985)
Parguaza Granite	Venezuela	Rb/Sr	1386 ± 28	Cited in Barrios et al. (1985)
Parguaza Granite	Venezuela	Rb/Sr	1486 ± 25	Bogotá (1981)
Los Pijiguaos Granite	Venezuela	Rb/Sr	1531 ± 39	Gaudette et al. (1978)
Parguaza Granite	Venezuela	Rb/Sr	1531 ± 39	Bogotá (1981)
Marieta Granite	Venezuela	Rb/Sr	1534 ± 13	Barrios y Rivas (1980)
Parguaza Granite	Venezuela	U/Pb	1545 ± 20	Gaudette et al. (1978)
Intrusive suite Alto Candeias	Brazil	U/Pb	1338-1346	Bettencourt et al. (1999)
Intrusive suite Teotônio	Brazil	U/Pb	1387 ± 16	Bettencourt et al. (1999)
Intrusive suite Santo Antônio	Brazil	U/Pb	1406 ± 32	Bettencourt et al. (1999)
Mucajaí Granite	Brazil	U/Pb	1544 ± 42	Gaudette et al. (1996)
Içana River (two- mica grainite)	Brazil	Pb/Pb	1521 ± 32	Almeida et al. (1997)
Papuri River granite	Brazil	U/Pb	1521 ± 13	Tassinari et al. (1996)
Charnockite Serra da Prata	Brazil	U/Pb	1564 ± 21	Fraga et al. (1997)
Surucucú Granite	Brazil	Rb/Sr	1583	Dall'Agnol et al. (1975)
Intrusive suite Serra da Providencia	Brazil	U/Pb	1606 -1532	Bettencourt et al. (1999)

557

7.2.2 Age relations with Nb-Ta, U-Th bearing minerals

Melcher et al., (2017) based on U–Pb isotopes in wodginite–ixiolite, CGM, rutile and cassiterite, estimated a mineralization age ranging from 1453 to 1277 Ma for their Colombian samples, although they did not report their exact provenances.

562 For other hand samples of LOC (2) and Venezuela were mineralogically
563 compared and rutile-(Nb,Ta) U-Pb ages are 1512 ± 12 Ma (Franco et al., 2021).

564 **7.3   Intraplate tectono-magmatic phenomena and paleogeographic**
565 **implications**

566 Intraplate tectono-magmatic phenomena are generally attributed to the ascent of
567 deep mantle plumes, arising from the core–mantle boundary. Mantle plumes are
568 consistent with experimental studies and mantle seismic tomography. In addition,
569 the assembly of supercontinents and their subsequent breakup are inferred to
570 relate to the arrival of mantle plumes (Ernst, 2014). The rising of mantle plumes
571 and/or asthenospheric melts results in tectonic and magmatic manifestations that
572 include crustal uplifts, continental rifting, the emplacement of anorogenic
573 magmas, and LIPs (large igneous provinces) on continents. Some of the most
574 significant global anorogenic magmatic rocks of Earth's history are recognized in
575 the period between 1300 and 1800 Ma (Ernst, 2014). For comparison, in
576 Laurentia, a distinctive A-type or "anorogenic" granites of ∼1.4 Ga age was
577 emplaced heterogeneous Proterozoic crust see Goodge and Vervoort (2006),
578 globally this magmatism according to conclusion in (Vigneresse, 2005) appears to
579 be unique because it requires a supercontinent with a zone of juvenile crust
580 surrounded by older cratons.

581 Huge Fe-Ti-V deposits hosted by anorogenic gabbro-anorthosite complexes, and
582 A-type granite related systems enriched in elements such as Sn, W, Cu, Zn, Bi,
583 Mo, U, and F are related to intraplate processes and mantle plume associated
584 magmatism (Pirajno, 2007).

585 Based on the distribution of fragments of LIP of distinct ages, Chaves and
586 Rezende (2019) have proposed a new reconstruction of Columbia (Nuna)
587 supercontinent. This reconstruction is shown in Figure 10, where purple and green
588 circles represent the thermal impact area promoted by 1.52 Ga and 1.38 Ga
589 mantle plume activity, recorded by volcanic mafic dykes and sills (LIP fragments).
590 The red circle in (Figure 10) corresponds to the studied area in the NW Amazon
591 Craton, which probably suffered partial melting generating A-type granites and
592 associated pegmatites with an age comparable to the one of mantle plumes.

593

594
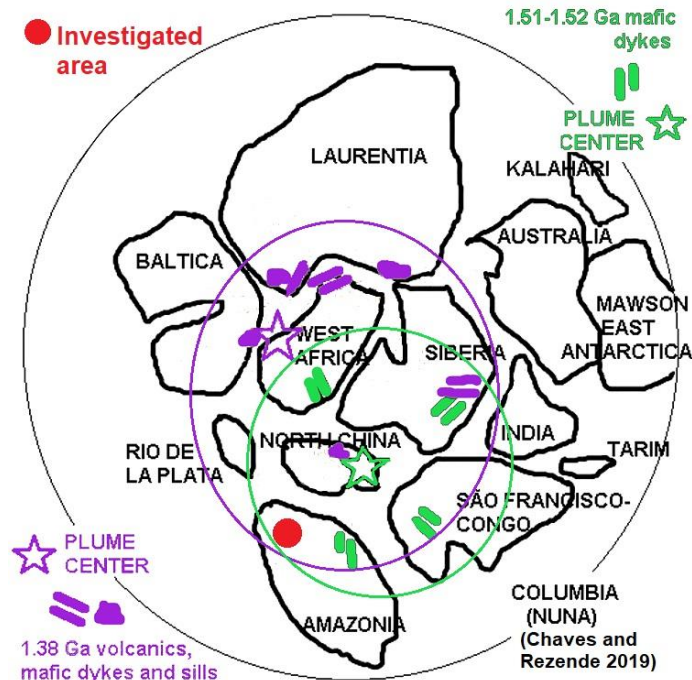
Figure 10. Columbia (Nuna) supercontinent reconstructed after Chaves and Rezende (2019). Purple and green circles represent the thermal impact area promoted by 1.52 Ga and 1.38 Ga mantle plume activity, recorded by their associated LIP fragments (volcanic, mafic dykes and sills). The red dot corresponds to the study area in the NW-Amazon Craton.

8   Conclusions

The monazite ages obtained by EPMA and LA-ICP-MS dating are in the same range for LOC (5) and (6) confirm that EPMA may be a useful tool to establish the crystallization age of monazite crystals poor in initial Pb. The high U, Th and radiogenic Pb contents and lack of inclusions and zonations of the homogeneous monazite crystals may make them suitable as internal standard material, however it would be necessary to find their primary source rocks, since there are age variations between the samples and the monazite grains from various primary sources may be in the same colluvial deposit.

The two age ranges suggest at least two enrichment events related with felsic intrusions and possibly associated pegmatites. The oldest ca. 1527 Ma processes forming CGM and the youngest of ca. 1346-1390 Ma forming REE and U-Th bearing minerals and in low proportion rutile-(Nb,Ta) and CGM.

The several kinds of ore minerals found in the three localities suggest different enrichment cycles linked to Mesoproterozoic magmatism. The Nb, Ta, U, Th and REE mineralizations may be result of pegmatitic phases of 1.52 Ga and 1.38 Ga anorogenic granitic magmatism triggered by mantle plumes affecting the Columbia (Nuna) supercontinent.

9 Acknowledgment

10 References

Aarden, H., Davidson, M., 1977. Minerales de estaño, niobio, tántalo y titanio en la zona del Cano Aguamena, Estado Bolívar, analizados con microsonda de electrones, in: Memorias V Congreso Geológico Venezolano. Caracas, pp. 919–940.

Almeida, F.F.M. de, Flasui, Y., Brito-Neves, B.B. de, Fuck, R.., 1981. Brazilian structural provinces: an introduction. Earth Sci. Rev. 17, 1–29.

Amaral, G., 1974. Geologia pré-cambriana da região Amazônica.

Barrios, F., y Rivas, D., 1980. Reconocimientogeocronológico del Territorio Federal Amazonas, Venezuela. Bol. Soc. Venez. Geol. 21: 1-12.

Barrios, F., Cordani, H., y Kasawachita, K., 1985a.Caracterización Geocronológica del T.F. Amazonas,Venezuela. En VI Cong. Geol. Venezolano, 3: 1.432-1.480.

Barrios, F., Rivas, D., Cordani, U., and Kawashita, K.1985b. Geocronología del Territorio Federal Amazonas.In: Memoria I Simposium Amazónico, Puerto Ayacucho,Venezuela. Bol. Geol., Publ. Esp., 10: 22-31.

Bettencourt, J.S., Tosdal, R.M., Leite, W.B., Payolla, B.L., 1999. Mesoproterozoic rapakivi granites of the Rondoˆnia Tin Province , southwestern border of the Amazonian craton , Brazil — I . Reconnaissance U – Pb geochronology and regional implications 95, 41–67.

Bonilla-Pérez, A., Frantz, J.C., Charão-Marques, J., Cramer, T., Franco-Victoria, J.A., Mulocher, E., Amaya-Perea, Z., 2013. Petrography, geochemistry and geochronology of Parguaza granite in Colombia. Bol. Geol. 35.

Bonilla, A., Cramer, T., Poujol, M., Cano, H., Franco, J.A., Amaya, Z., 2019. Petrografía, geoquímica y geocronología U/Pb en circones de rocas ígneas y metamórficas a lo largo del Río Cuiarí en el sur del Departamento de Guainía, Colombia. Boletín Geol. 41, 55–84. https://doi.org/10.18273/revbol.v41n1-2019003

Bonilla, A., Frantz, J.C., Charão-Marques, J., Cramer, T., Franco, J.A., Amaya,

Z., 2016. Rapakivi magmatism in the middle Inirida Basin, Guainía deparment, Colombia. Bol. Geol. 38. https://doi.org/10.18273/revbol.v38n1-2016001

Bonilla, Amed (2019). Origen y evolución de los granitoides proterozoicos del Oriente Colombiano, noroeste del cratón amazónico.Universidad Nacional de Colombia, Doctoral thesis, Bogotá

Bonilla Perez, A., Franco, J.A., Cramer, T., Poujol, M., Cogné, N., Nachtergaele, S., De Grave, J., 2020. Apatite LA-ICP-MS U–Pb and fission-track geochronology of the Caño Viejita gabbro in E-Colombia: Evidence for Grenvillian intraplate rifting and Jurassic exhumation in the NW Amazonian Craton. J. South Am. Earth Sci. 98, 102438. https://doi.org/10.1016/j.jsames.2019.102438

Bonin, B., 2007. A-type granites and related rocks : Evolution of a concept , problems and prospects 97, 1–29. https://doi.org/10.1016/j.lithos.2006.12.007

Celada, C., Garzón, M., Gómez, E., Khurama, S., López, J., Mora, M., Navas, O., Pérez, R., Vargas, O., Westerhof, P., 2006. Potencial de Recursos Minerales en el Oriente Colombiano: Compilación y Análisis de la Información Geológica Disponible. INGEOMINAS, Bogotá - Colombia.

Černý, P., 1991. Rare-element granitic pegmatites. Part 1: Anatomy and internal evolution of pegmatite deposits. Geosci. Canada 18, 49–67.

Černý, P., Blevin, P.L., Cuney, M., London, D., 2005. Granite-related ore deposits. Econ. Geol. 100th Anniv. Vol. 337–370.

Černý, P., Ercit, T.S., 2005. The classification of granitic pegmatites revisited. Can. Mineral. 43, 2005–2026. https://doi.org/10.2113/gscanmin.43.6.2005

Cerný, P., London, D., Novák, M., 2012. Granitic Pegmatites as Reflections of Their Sources. Elements 8, 289–294. https://doi.org/10.2113/gselements.8.4.289

Chappell, B.W., White, A.J.R., 2001. Two contrasting granite types: 25 years later. Aust. J. Earth Sci. 48, 489–499. https://doi.org/10.1046/j.1440-0952.2001.00882.x

Chappell, B.W., White, A.J.R., 1974. Two contrasting granite types. Pacific Geol. 8, 173–174.

Chaves, A. de O., Oliveira, E.K. de, Garcia, L.R.A., 2013. Desenvolvimento do método de datação química U-Th-Pb de monazita por microssonda eletrônica na UFMG. Geonomos 21, 13–18. https://doi.org/10.18285/geonomos.v21i2.268

Chaves, A. de O. and Rezende, C. R., 2019, Fragments of 1.79-1.75 Ga Large Igneous Provinces in reconstructing Columbia (Nuna): a Statherian supercontinentsuperplume coupling?. EPISODES, v. 42, p. 55-67.

Cordani, U.G., Sato, K., Sproessner, W., Santos Fernandes, F., 2016. U-Pb zircon ages of rocks from the Amazonas Territory of Colombia and their bearing on the tectonic history of the NW sector of the Amazonian Craton. Brazilian J. Geol. 46, 5–35. https://doi.org/10.1590/2317-4889201620150012

705 Dall'Agnol, R., Costi, H.T., Leite, A.A. da S., de Magalhães, M.S., Teixeira, N.P.,
706   1999. Rapakivi granites from Brazil and adjacent areas. Precambrian Res.
707   95, 9–39. https://doi.org/10.1016/S0301-9268(98)00125-9

708 Deer, W.A., Howie, R.A., Zussman, J., 2013. An Introduction to the Rock-Forming
709   Minerals. Mineralogical Society of Great Britain and Ireland.
710   https://doi.org/10.1180/DHZ

711 Dill, H.G., 2015. Pegmatites and aplites: Their genetic and applied ore geology.
712   Ore Geol. Rev. 69, 417–561.
713   https://doi.org/10.1016/j.oregeorev.2015.02.022

714 Dill, H.G., Melcher, F., Füßl, M., Weber, B., 2006. Accessory minerals in
715   cassiterite: A tool for provenance and environmental analyses of colluvial–
716   fluvial placer deposits (NE Bavaria, Germany). Sediment. Geol. 191, 171–
717   189. https://doi.org/10.1016/j.sedgeo.2006.03.022

718 Eby, G.N., 1990. The A-type granitoids: A review of their occurrence and chemical
719   characteristics and speculations on their petrogenesis. Lithos 26, 115–134.
720   https://doi.org/10.1016/0024-4937(90)90043-Z

721 Engi, M., 2017, Petrochronology based on REE-Minerals: Monazite, Allanite,
722   Xenotime, Apatite: Reviews in Mineralogy and Geochemistry, v. 83, p. 365
723   LP – 418.

724 Ernst, R.E., 2014. Large Igneous Provinces (1st edition). Cambridge University
725   Press, Cambridge, p. 653.

726 Franco Victoria, J.A., 2015. Contribución a la geología histórica del Oriente
727   Colombiano: Proveniencia de minerales metálicos con Nb, Ta, Mn, Fe, Ti,
728   Sn y W, de un depósito laterizado, en cercanías a la Comunidad Indígena
729   de Cachicamo, al NE del Departamento del Vichada. Universidad Nacional
730   de Colombia, Tesis de Maestria, Bogotá, Bogotá.

731 Franco Victoria, J.A., Cramer, T., Bonilla-Pérez, A., Castañeda, A.J., Poujol, M.,
732   Amaya-Perea, Z., 2021. Mineralogía y geocronología de rutilo-(Nb,Ta)
733   relacionado a casiterita y columbita-tantalita provenientes de rocas
734   Mesoproterozoicas del Cratón Amazónico cerca de Cachicamo, Colombia.
735   Bol. Geol. 43, 99–126. https://doi.org/10.18273/revbol

736 Frost, B.R., Frost, C.D., 2014. Essentials of igneous and metamorphic petrology.
737   Cambridge University Press.

738 Galvis Vergara, J., Hugett, A., Ruge, P., 1979a. Proyecto Radargramétrico del
739   Amazonas. La Amazonía Colombiana y sus recursos. Inst. Geográfico
740   Agustín Codazzi, i 33–91.

741 Galvis Vergara, J., Huguett, A., Ruge, P., 1979b. Geología de la Amazonía
742   Colombiana. Boletín Geológico, Boletín Geológico 22, 3–86.

743 Gandhi, S.M., Sarkar, B.C., 2016. Essentials of Mineral Exploration and
744   Evaluation. Elsevier, Amsterdam, p. 408. https://doi.org/10.1016/B978-0-12-
745   805329-4.00008-9

746 Gansser, A., 1974. The Roraima Problem (South America). Verhandl. Naturf.
747   Ges., Basel 84, 80–100.

748 Gansser, A., 1954. The Guiana Shield (S. America) Geological Observations.

749   Eclog. Geol. Helvet 47, 77–112.

750   Gasquet D, Bertrand JM, Paquette J-L, Lehmann J, Ratzov G, De Ascencao
751   Guedes R, Tiepolo M, Boullier AM, Scaillet S, Nomade S, (2010) Miocene to
752   Messinian deformation and hydrothermalism in the Lauzière Massif (French
753   Western Alps): new U-Th-Pb and Argon ages. Bulletin de la Société
754   Géologique de France 181:227-241.

755   Gaudette, H.E., Mendoza, V.S., Hurley, P.M., Fairbairn, H.W., 1978. Geology and
756   age of the Parguaza rapakivi granite, Venezuela. Geol. Soc. Am. Bull. 89,
757   1335–1340.   https://doi.org/10.1130/0016-
758   7606(1978)89<1335:GAAOTP>2.0.CO;2

759   Gaudette, H.E., Olszewski, W.J., 1985. Geochronology of the basement rocks,
760   Amazonas territory, Venezuela and Tectonic evolution of the western Guiana
761   Shield. Geol. en Mijnb. 64, 131–143.

762   Ginsburg, A.I., Timofeyev, I.N., Feldman, L.G., 1979. Principles of geology of the
763   granitic pegmatites. Nedra, Moscow.

764   Gómez Tapias, J., Nivia Guevara, Á., Montes Ramírez, N.E., Almanza Meléndez,
765   M.F., Alcárcel Gutiérrez, F.A., Madrid Montoya, C.A., 2015. Compilando la
766   geología de Colombia: Una visión a 2015. Imprenta Nacional de Colombia,
767   Bogotá.

768   Goodge, J.W., & Vervoort, J.D., 2006. Origin of Mesoproteroizoic A-type granites
769   in Laurentia: Hf isotope evidence. Earth and Planetary Science Letters, 243,
770   pp. 711- 731.

771   Henderson, P., 1984, Chapter 1 - General Geochemical Properties and
772   Abundances of the Rare Earth Elements, in Henderson, P. B. T.-D. in G. ed.,
773   Rare Earth Element Geochemistry: Elsevier, p. 1–32.

774   Herrera-Bangerter, G.C., 1989. Die proterozoischen Rapakivigranite von El
775   Parguaza (südliches Venezuela) - Dissertation. Universität Zürich.

776   Hiess, J., Condon, D.J., McLean, N., Noble, S.R., 2012. 238U/235U Systematics
777   in Terrestrial Uranium-Bearing Minerals. Science (80-.). 335, 1610–1614.
778   https://doi.org/10.1126/science.1215507

779   Huguett, A., Galvis, J., Ruge, P., 1979. La Amazonía Colombiana y sus recursos.
780   Geología, La Amazonía Colombiana y sus recursos. Proyecto
781   Radargramétrico del Amazonas. Bogotá.

782   Ibañez-Mejia, M., Ruiz, J., Valencia, V.A., Cardona, A., Gehrels, G.E., Mora, A.R.,
783   2011. The Putumayo Orogen of Amazonia and its implications for Rodinia
784   reconstructions: New U–Pb geochronological insights into the Proterozoic
785   tectonic evolution of northwestern South America. Precambrian Res. 191,
786   58–77. https://doi.org/10.1016/j.precamres.2011.09.005

787   Itano, K., Iizuka, T., Chang, Q., Kimura, J. I., and Maruyama, S., 2016, U–Pb
788   chronology and geochemistry of detrital monazites from major African rivers:
789   Constraints on the timing and nature of the Pan-African Orogeny:
790   Precambrian Research, v. 282, p. 139–156.

791   Itano, K., Iizuka, T., and Hoshino, M., 2018, REE-Th-U and Nd isotope
792   systematics of monazites in magnetite- and ilmenite-series granitic rocks of
793   the Japan arc: Implications for its use as a tracer of magma evolution and

794   detrital provenance: Chemical Geology, v. 484, p. 69–80.

795   Jercinovic, M.J., Williams, M.L., Lane, E.D., 2008. In-situ trace element analysis
796   of monazite and other fine-grained accessory minerals by EPMA. Chem.
797   Geol. 254, 197–215. https://doi.org/10.1016/j.chemgeo.2008.05.016

798   Kroonenberg, S.B., 2019. The Proterozoic Basement of the Western Guiana
799   Shield and the Northern Andes, in: Cediel, F., Shaw, R.P. (Eds.), Geology
800   and Tectonics of Northwestern South America. Springer International
801   Publishing, Cham, pp. 115–192. https://doi.org/10.1007/978-3-319-76132-
802   9_3

803   Kroonenberg, S.B., de Roever, E.W.F., Fraga, L.M., Reis, N.J., Faraco, T., Lafon,
804   J.-M., Cordani, U., Wong, T.E., 2016. Paleoproterozoic evolution of the
805   Guiana Shield in Suriname: A revised model. Netherlands J. Geosci. 95,
806   491–522. https://doi.org/10.1017/njg.2016.10

807   Larin, A. M., 2009, Rapakivi granites in the geological history of the earth. Part 1,
808   magmatic associations with rapakivi granites: Age, geochemistry, and
809   tectonic setting: Stratigraphy and Geological Correlation, v. 17, p. 235–258.

810   Laznicka, P., 2006. Giant Metallic Deposits - Future Sources of Industrial Metals.
811   Springer.

812   London, D., 2018. Ore-forming processes within granitic pegmatites. Ore Geol.
813   Rev. 101, 349–383. https://doi.org/10.1016/j.oregeorev.2018.04.020

814   London, D., Morgan, G.B., 2012. The Pegmatite Puzzle. Elements 8, 263–268.
815   https://doi.org/10.2113/gselements.8.4.263

816   López Isaza, J.A., 2012. Unidades, petrografía y composición química del
817   Complejo Migmatítico de Mitú en los alrededores de Mitú: Réplica. Boletín
818   Geol. 34.

819   López Isaza, J.A., Cramer, T., 2012. Ambiente geológico del complejo Mitú y
820   perspectivas de ocurrencias minerales de niobio y tantalio en el territorio
821   colombiano. Geol. Colomb. 37, 75–95.

822   López Isaza, J.A., Khurama, S., Bernal Vargas, L.E., Cuéllar, M.A., 2007. El
823   Complejo Mitú: una nueva perspectiva, in: Memorias Del XI Congreso
824   Colombiano de Geología. Sociedad Colombiana de Geología,
825   Bucaramanga, pp. 1–16.

826   López, J., Mora, B., Jiménez, D.M., Khurama, S., Marín, E., Obando, G., Páez,
827   T.I., Carrillo, L.E., Bernal, L., 2010. Cartografía Geológica y Muestreo
828   Geoquímico de las Planchas 297 – Puerto Inírida, 297 Bis – Merey Y 277
829   Bis – Amanaven, Departamento del Guainía. Ingeominas, Bogotá.

830   Ludwig, K.R., 2012. User´s manual for Isoplot 3.75 - A Geochronological Toolkit
831   for Microsoft Excel, Berkeley Geochronology Center Special Publication No.
832   5.

833   Ludwig, K.R., 2003. User's Manual for Isoplot 3.00 - A Geochronological Toolkit
834   for Microsoft Excel, Berkeley Geochronology Center Special Publication.

835   Magrini, D., Attanasio, D., Bracci, S., Cantisani, E., Prochaska, W., 2018.
836   Innovative application of portable X-ray fluorescence (XRF) to identify
837   Göktepe white marble artifacts. Archaeol. Anthropol. Sci. 10, 1141–1152.

838   https://doi.org/10.1007/s12520-016-0444-7

839   Mange, M.A., Wright, D.T. (Eds.), 2007. Heavy minerals in use, Developments in
840   Sedimentology, 58, Developments in Sedimentology, 58.

841   Mariño-Pardo, N., 2012. Potencial minero del Bajo Parguaza. Rev. Commod.
842   Venez. 2, 44–47.

843   Mariño, N., 2013. Coltán en Venezuela. Energía&Petróleo.

844   Melcher, F., Graupner, T., Gäbler, H.-E.E., Sitnikova, M., Oberthür, T., Gerdes,
845   A., Badanina, E., Chudy, T., 2017. Mineralogical and chemical evolution of
846   tantalum–(niobium–tin) mineralisation in pegmatites and granites. Part 2:
847   Worldwide examples (excluding Africa) and an overview of global
848   metallogenetic patterns. Ore Geol. Rev. 89, 946–987.
849   https://doi.org/10.1016/j.oregeorev.2016.03.014

850   Montel, J.-M., Razafimahatratra, D., de Parseval, P., Poitrasson, F., Moine, B.,
851   Seydoux-Guillaume, A.-M., Pik, R., Arnaud, N., and Gibert, F., 2018, The
852   giant monazite crystals from Manangotry (Madagascar): Chemical Geology,
853   v. 484, p. 36–50.

854   Montel, J., Foret, S., Veschambre, M., Nicollet, C., and Provost, A., 1996,
855   Chemical Electron microprobe dating of monazite: v. 1.

856   Mottana, A., Crespi, R., Liborio, G., Prinz, M., Harlow, G. E., and Peters, J., 1978,
857   Simon and Schuster's guide to rocks and minerals: Simon and Schuster.

858   Paquette J-L, Tiepolo M, (2007) High resolution (5 µm) U-Th-Pb isotopes dating
859   of monazite with excimer laser ablation (ELA)-ICPMS. Chemical Geology
860   240:222-237.

861   Perkins, D., 2014. Mineralogy, 3rd ed. Pearson Educación, Harlow.

862   Pinheiro, S.S., Fernández, P.E.C.A. Pereira, E.., Vasconcelos, E.., Pinto, A..,
863   Montalvão, R.M.., Issler, R.., Dall'Agnol, R., Teixeira, W., Fernández, C.A.C.,
864   1976. Geología - Projeto Radar na Amazônia. Folha NA.19-Pico da Neblina,
865   in: Levantamento de Recursos Naturais- Vol 11. pp. 19–137.

866   Pirajno, F., 2007, Chapter 8.3 Ancient to Modern Earth: The Role of Mantle
867   Plumes in the Making of Continental Crust, in Kranendonk, M. J. Van,
868   Smithies, R. H., and Bennett, V. C. eds., Developments in Precambrian
869   Geology:, p. 1037–1064.

870   Pirajno, F., 2009, Hydrothermal Processes and Mineral Systems: Dordrecht,
871   Springer Netherlands, 1273 p.

872   Pommier, A., Cocherie, A., Legendre, O., 2004. EPMA Dating User'Manual, V.
873   1.01: Age Calculation from Electron Probe Microanalyser Measurements of
874   U–Th–Pb. Brgm, Orleans.

875   Priem, H.N.A., Andriessen, P.A.M., Boelrijk, N.A.I.M., Boorder, H. de, Hebeda,
876   E.H., Huguett, A., Verdurmen, E.A.T., Verschure, R.H., 1982.
877   Geochronology of the Precambrian in the Amazonas Region of Southeastern
878   Colombia (Western Guiana Shield). Geol. en Mijnb. 61, 229–242.

879   Poujol M, Pitra P, Van Den Driessche J, Tartèse R, Ruffet G, Paquette J-L, Poilvet
880   J-C (2017) Two-stage partial melting during the Variscan extensional
881   tectonics (Montagne Noire, France). Int J Earth Sci 106:477-500. doi:

882   10.1007/s00531-016-1369-1.

883 Reed, S.J.B., 2005. Electron Microprobe Analysis and Scanning Electron
884   Microscopy in Geology, Electron Microprobe Analysis and Scanning Electron
885   Microscopy in Geology. Cambridge University Press, Cambridge.
886   https://doi.org/10.1017/CBO9780511610561

887 Santos, J.O.S., 2003. Geotectônica dos Escudos das Guianas e Brasil-Central.
888   Geol. Tectônica e Recur. Minerais do Bras. 4, 169–195.

889 Santos, J.O.S., Hartmann, L.A., Gaudette, H.E., Groves, D.I., Mcnaughton, N.J.,
890   Fletcher, I.R., 2000. A new understanding of the Provinces of the Amazon
891   Craton based on Integration of Field Mapping and U-Pb and Sm-Nd
892   Geochronology. Gondwana Res. 3, 453–488. https://doi.org/10.1016/S1342-
893   937X(05)70755-3

894 Santos, J.O.S., Potter, P.E., Reis, N.J., Hartmann, L.A., Fletcher, I.R.,
895   McNaughton, N.J., 2003. Age, source, and regional stratigraphy of the
896   Roraima Supergroup and Roraima-like outliers in northern South America
897   based on U-Pb geochronology. Geol. Soc. Am. Bull. 115, 331–348.
898   https://doi.org/10.1130/0016-7606(2003)115<0331:ASARSO>2.0.CO;2

899 Santos, J.O.S., Rizzotto, G.J., Potter, P.E., McNaughton, N.J., Matos, R.S.,
900   Hartmann, L.A., Chemale, F., Quadros, M.E.S., 2008. Age and
901   autochthonous evolution of the Sunsás Orogen in West Amazon Craton
902   based on mapping and U-Pb geochronology. Precambrian Res. 165, 120–
903   152. https://doi.org/10.1016/j.precamres.2008.06.009

904 SERVICIO GEOLÓGICO COLOMBIANO. 2013. Cartografía geológica y
905   muestreo geoquímico de las planchas 201 BIS, 201, 200 Y 199
906   Departamento de Vichada. Memoria explicativa. Bogota

907 Scherrer, N.C., Eng, M., Gnos, E., Jakob, V., Liechti, A., 2000, Monazite analysis;
908   from sample preparation to microprobe age dating and REE quantification.
909   Schweizer Mineralogische und Petrographische Mitteilungen, v. 80, p. 93-
910   105.

911 Sial, A.N., Bettencourt, J.S., Campos, C.P. De, Ferreira, V.P. (Eds.), 2011.
912   Granite-related ore deposits, Geological Society, London, Special
913   Publications. Geological Society, London, London.
914   https://doi.org/10.1144/SP350.1

915 Sun, S.–., McDonough, W.F., 1989. Chemical and isotopic systematics of oceanic
916   basalts: implications for mantle composition and processes. Geol. Soc.
917   London, Spec. Publ. 42, 313–345.
918   https://doi.org/10.1144/GSL.SP.1989.042.01.19

919 Suzuki, K., and Kato, T., 2008, CHIME dating of monazite, xenotime, zircon and
920   polycrase: Protocol, pitfalls and chemical criterion of possibly discordant age
921   data: Gondwana Research, v. 14, p. 569–586.

922 Tassinari, C.C.G., Macambira, M.J.B., 1999. Geochronological provinces of the
923   Amazonian Craton. Episodes 22, 174–182.
924   https://doi.org/10.1080/00206819709465329

925 Vermeesch, P., 2018. IsoplotR: A free and open toolbox for geochronology.
926   Geosci. Front. 9, 1479–1493. https://doi.org/10.1016/j.gsf.2018.04.001

927 Vigneresse, J.L., 2005,The specific case of the Mid-Proterozoic rapakivi granites
928   and associated suite within the context of the Columbia supercontinent,
929   Precambrian Research, Volume 137, Issues 1–2, , Pages 1-34, ISSN 0301-
930   9268, https://doi.org/10.1016/j.precamres.2005.01.001.

931 Williams, M.L., Jercinovic, M.J., Hetherington, C.J., 2007, Microprobe Monazite
932   Geochronology : Understanding Geologic Processes by Integrating
933   Composition   and   Chronology.
934   https://doi.org/10.1146/annurev.earth.35.031306.140228

935 Williams, M. L., Jercinovic, M. J., Mahan, K. H., and Dumond, G., 2017, Electron
936   Microprobe Petrochronology: Reviews in Mineralogy and Geochemistry, v.
937   83, p. 153–182.

938 Winter, J. D., 1972, Introduction to Igneous and Metamorphic Petrology: Upper
939   Saddle River, New Jersey, Prentice Hall, 697 p.

940 Zhu, X. and O'Nions, R. 1999, Monazite chemical composition: some implications
941   for   monazite   geochronology. Contrib   Mineral   Petrol, 137, 351–363.
942   https://doi.org/10.1007/s004100050555

943
944

11 Annex, supplementary tables

Annex A. Supplementary table of operating conditions for the LA-ICP-MS equipment (GeOHeLiS Platform).

Laboratory & Sample Preparation

Laboratory name	GeOHeLiS Platform, University of Rennes, Rennes, France
Sample type/mineral	Monazite
Sample preparation	Separated grain mounted in epoxy pucks

Laser ablation system

Make, Model & type	ESI NWR193UC, Excimer
Ablation cell	ESI NWR TwoVol2
Laser wavelength	193 nm
Pulse width	< 5 ns
Fluence	5 J/cm^2
Repetition rate	3Hz
Spot size	8 µm
Sampling mode / pattern	Single spot
Carrier gas	100% He, Ar make-up gas and N2 (3 ml/mn) combined using in-house smoothing device
Background collection	20 seconds
Ablation duration	60 seconds
Wash-out delay	15 seconds
Cell carrier gas flow (He)	0.75 l/min

ICP-MS Instrument

Make, Model & type	Agilent 7700x, Q-ICP-MS
Sample introduction	Via conventional tubing
RF power	1350W
Sampler, skimmer cones	Ni
Extraction lenses	X type
Make-up gas flow (Ar)	0.85 l/min
Detection system	Single collector secondary electron multiplier
Data acquisition protocol	Time-resolved analysis
Scanning mode	Peak hopping, one point per peak
Detector mode	Pulse counting, dead time correction applied, and analog mode when signal intensity > ~ 10^6 cps
Masses measured	^{204}(Hg + Pb), ^{206}Pb, ^{207}Pb, ^{208}Pb, ^{232}Th, ^{238}U
Integration time per peak	10-30 ms
Sensitivity / Efficiency	22000 cps/ppm Pb (50µm, 10Hz)

Data Processing

Gas blank	20 seconds on-peak
Calibration strategy	Moacir monazite standard used as primary reference material, Managoutry monazite used as secondary reference material (quality control)

Reference Material info	Moacir (Gasquet et al., 2010)
	Manangoutry (Paquette and Tiepolo, 2007)
Data processing package used	GLITTER ® (van Achterbergh et al., 2001)
Mass discrimination	Standard-sample bracketing with $^{207}Pb/^{206}Pb$, $^{206}/^{238}U$, $^{208}Pb/^{232}Th$ normalized to reference material Moacir
Common Pb correction	No common Pb correction
Uncertainty level and propagation	Ages are quoted at 2 sigma absolute, propagation is by quadratic addition according to Horstwood et al. (2016). Reproducibility and age uncertainty of reference material are propagated.
Quality control / Validation	Manangoutry : 548 ± 6 Ma (MSWD=0.98 ; n=11)

Annex B. EPMA mineral chemistry data of monazite crystals from the localities Espina Hills LOC (4); San José LOC (5) and Barranquilla LOC (6) and ages calculated using Th, U and Pb contents. All elements are expressed as main oxides measure in weighted percent (wt.%) independently of their real oxidation state.

Sample	Analysis point/ oxide	P₂O₅	SiO₂	ThO₂	UO₂	Y₂O₃	La₂O₃	Ce₂O₃	Pr₂O₃	Nd₂O₃	Sm₂O₃	Gd₂O₃	Dy₂O₃	CaO	PbO	Total	U (ppm)	2σ %	Th (ppm)	2σ %	Pb (ppm)	2σ %	Age (Ma)	2σ (abs)
LOC4	1	27.99	1.05	8.65	0.27	1.38	10.83	30.00	3.04	10.75	2.90	1.18	0.64	1.49	0.57	100.73	1896	5.3	76016	1	5291	1.9	**1393**	45
	2	26.28	1.07	8.56	0.26	1.51	10.54	29.74	3.02	11.02	2.97	1.28	0.61	1.46	0.56	98.86	1813	5.5	75225	1	5198	1.9	**1387**	45
	3	26.32	1.16	8.14	0.18	1.45	11.00	30.23	3.04	11.27	2.77	1.23	0.60	1.13	0.51	99.02	1131	8.8	71534	1	4734	2.1	**1366**	48
	4	27.30	1.14	8.33	0.20	1.40	11.10	30.48	3.16	11.31	2.83	1.28	0.47	1.22	0.53	100.73	1297	7.7	73204	1	4920	2.0	**1378**	47
	5	26.08	1.37	8.51	0.18	1.41	11.00	30.23	3.25	11.52	2.60	1.19	0.51	0.94	0.55	99.32	1111	9.0	74786	1	5106	2.0	**1412**	47
	6	25.55	1.62	8.09	0.18	1.29	11.46	30.74	3.23	11.81	2.49	1.21	0.45	0.80	0.51	99.42	1134	8.8	71095	1	4734	2.1	**1374**	48
	7	26.15	1.04	8.65	0.28	1.48	10.71	29.31	2.96	10.86	2.89	1.21	0.68	1.45	0.58	98.23	1984	5.0	76016	1	5384	1.9	**1412**	45
LOC5	1	26.26	1.26	12.23	0.46	1.53	9.63	27.55	2.86	9.16	3.26	1.49	0.58	2.02	0.89	99.18	3371	3.0	107477	1	8262	1.2	**1502**	36
	2	27.61	1.19	11.95	0.44	1.22	9.95	28.21	2.95	9.49	3.40	1.52	0.50	1.91	0.87	101.21	3210	3.1	105017	1	8076	1.2	**1506**	37
	3	25.88	1.15	10.49	0.40	1.29	10.10	28.86	3.01	9.56	3.53	1.53	0.53	1.65	0.79	98.75	2939	3.4	92186	1	7334	1.4	**1549**	40
	4	26.40	1.06	9.56	0.35	0.98	10.49	30.38	3.08	9.93	3.48	1.46	0.32	1.52	0.69	99.69	2551	3.9	84013	1	6405	1.6	**1495**	42
	5	25.10	1.23	11.04	0.44	1.14	10.42	29.41	2.87	9.38	3.09	1.40	0.50	1.78	0.84	98.64	3261	3.1	97020	1	7798	1.3	**1556**	39
	6	25.39	1.20	11.14	0.44	1.20	9.83	27.86	2.88	9.66	3.34	1.36	0.49	1.85	0.83	97.47	3255	3.1	97898	1	7705	1.3	**1527**	38
	7	27.96	0.77	4.10	0.21	1.44	13.58	33.57	3.15	10.08	1.79	0.77	0.39	0.59	0.32	98.71	1578	6.3	36004	1.00	2933	3.41	**1529**	77
	8	27.49	1.34	5.86	0.27	1.55	12.35	32.03	3.31	10.95	2.22	1.10	0.37	0.72	0.45	100.00	2026	4.9	51506	1.00	4140	2.42	**1530**	59
LOC6	1	23.43	2.27	10.89	0.37	2.11	8.36	27.95	3.43	12.98	3.34	1.39	0.43	0.73	0.79	98.46	2652	3.8	95701	1	7334	1.4	**1514**	39
	2	24.17	2.20	10.72	0.34	2.15	8.39	27.91	3.41	12.85	3.40	1.28	0.44	0.73	0.78	98.77	2397	4.2	94207	1	7241	1.4	**1529**	40
	3	24.88	2.44	11.49	0.38	2.18	8.46	27.97	3.47	12.72	3.51	1.31	0.37	0.72	0.85	100.73	2707	3.7	100974	1	7891	1.3	**1547**	38
	4	24.27	2.08	10.07	0.35	1.94	8.60	28.78	3.22	13.15	3.57	1.33	0.32	0.69	0.74	99.10	2522	4.0	88495	1	6869	1.5	**1529**	41
	5	24.89	2.05	9.95	0.34	2.02	8.54	28.28	3.48	13.13	3.56	1.36	0.47	0.71	0.73	99.51	2441	4.1	87441	1	6777	1.5	**1530**	42
	6	25.27	2.12	10.12	0.34	2.12	8.65	28.19	3.38	13.02	3.66	1.31	0.52	0.68	0.74	100.11	2431	4.1	88935	1	6869	1.5	**1527**	41
	7	25.30	1.50	9.81	0.35	2.19	8.51	28.21	3.37	12.54	3.69	1.59	0.41	1.10	0.71	99.29	2537	3.9	86210	1	6591	1.5	**1503**	42

Sample	Analysis point/ oxide	P_2O_5	SiO_2	ThO_2	UO_2	Y_2O_3	La_2O_3	Ce_2O_3	Pr_2O_3	Nd_2O_3	Sm_2O_3	Gd_2O_3	Dy_2O_3	CaO	PbO	Total	U (ppm)	2σ %	Th (ppm)	2σ %	Pb (ppm)	2σ %	Age (Ma)	2σ (abs)
8		24.89	1.87	11.07	0.39	2.06	8.56	26.92	3.22	12.71	3.55	1.50	0.52	1.17	0.81	99.24	2819	3.5	97283	1	7519	1.3	**1521**	39
9		24.74	1.53	9.62	0.31	1.90	8.59	27.62	3.26	13.33	4.00	1.68	0.43	1.08	0.71	98.80	2195	4.6	84541	1	6591	1.5	**1548**	43
10		25.66	1.76	10.61	0.34	2.08	8.55	27.08	3.39	12.77	3.82	1.46	0.39	1.27	0.77	99.95	2404	4.2	93241	1	7148	1.4	**1524**	40

1

2   Annex C. LA-ICP-MS U/Th/Pb isotopic data of monazite crystals from Espina Hills LOC (4), San José LOC (5) and Barranquilla LOC (6).

Points of ablation	$^{208}Pb/^{232}Th$	PropErr2σAbs	$^{206}Pb/^{238}U$	PropErr2σAbs	Age $^{206}Pb/^{238}U$	PropErr2σAbs	Age $^{208}Pb/^{232}Th$	PropErr2σAbs
Mnz_Loc (4) p1	0.0670	0.0051	0.230	0.016	1327	22	1311	14
Mnz_Loc (4) p2	0.0660	0.0050	0.230	0.016	1327	26	1291	16
Mnz_Loc (4) p3	0.0716	0.0054	0.238	0.017	1377	22	1397	17
Mnz_Loc (4) p4	0.0685	0.0052	0.239	0.017	1380	19	1339	15
Mnz_Loc (4) p5	0.0673	0.0051	0.229	0.016	1322	22	1316	16
Mnz_Loc (4) p6	0.0697	0.0052	0.233	0.016	1352	29	1361	17
Mnz_Loc (4) p7	0.0690	0.0053	0.238	0.016	1371	22	1350	16
Mnz_Loc (4) p8	0.0687	0.0053	0.239	0.017	1379	22	1343	16
Mnz_Loc (4) p9	0.0636	0.0051	0.230	0.016	1325	55	1245	26
Mnz_Loc (4) p10	0.0676	0.0052	0.233	0.016	1347	30	1321	19
Mnz_Loc (4) p11	0.0637	0.0049	0.231	0.016	1334	28	1248	15
Mnz_Loc (4) p12	0.0683	0.0052	0.233	0.016	1345	27	1334	20
Mnz_Loc (4) p13	0.0664	0.0051	0.232	0.016	1340	23	1298	16
Mnz_Loc (4) p14	0.0696	0.0053	0.238	0.016	1374	22	1360	16
Mnz_Loc (4) p15	0.0686	0.0053	0.238	0.016	1373	23	1341	18
Mnz_Loc (4) p16	0.0683	0.0052	0.240	0.017	1383	22	1335	16
Mnz_Loc (4) p17	0.0711	0.0054	0.244	0.017	1406	21	1388	16
Mnz_Loc (4) p18	0.0662	0.0051	0.231	0.016	1331	26	1294	17
Mnz_Loc (4) p19	0.0672	0.0051	0.236	0.017	1356	30	1314	16

Mnz_Loc (4) p20	0.0673	0.0051	0.236	0.016	1360	20	1315	15
Mnz_Loc (4) p21	0.0703	0.0054	0.243	0.017	1399	20	1371	16
Mnz_Loc (4) p22	0.0679	0.0052	0.235	0.016	1361	19	1326	13
Mnz_Loc (5) p1	0.0801	0.0036	0.265	0.011	1511	55	1556	67
Mnz_Loc (5) p2	0.0796	0.0036	0.265	0.010	1513	53	1547	67
Mnz_Loc (5) p3	0.0824	0.0037	0.276	0.011	1569	57	1599	70
Mnz_Loc (5) p4	0.0801	0.0037	0.268	0.011	1523	56	1556	69
Mnz_Loc (5) p5	0.0761	0.0034	0.258	0.010	1474	53	1482	64
Mnz_Loc (5) p6	0.0787	0.0035	0.264	0.010	1505	53	1530	66
Mnz_Loc (5) p7	0.0753	0.0034	0.256	0.011	1465	54	1468	63
Mnz_Loc (5) p8	0.0764	0.0034	0.255	0.010	1461	52	1488	64
Mnz_Loc (5) p9	0.0783	0.0035	0.259	0.010	1482	53	1523	65
Mnz_Loc (5) p10	0.0767	0.0034	0.259	0.010	1481	51	1492	64
Mnz_Loc (5) p11	0.0828	0.0037	0.273	0.011	1553	58	1606	69
Mnz_Loc (5) p12	0.0808	0.0036	0.270	0.011	1540	55	1570	67
Mnz_Loc (5) p13	0.0827	0.0037	0.275	0.011	1560	58	1606	69
Mnz_Loc (5) p14	0.0809	0.0036	0.273	0.011	1549	55	1571	67
Mnz_Loc (6) p1	0.0784	0.0035	0.262	0.011	1499	56	1525	66
Mnz_Loc (6) p2	0.0780	0.0035	0.260	0.010	1488	53	1517	65
Mnz_Loc (6) p3	0.0771	0.0034	0.259	0.011	1481	55	1500	64
Mnz_Loc (6) p4	0.0851	0.0038	0.281	0.011	1596	57	1649	70
Mnz_Loc (6) p5	0.0817	0.0036	0.273	0.011	1554	55	1587	68
Mnz_Loc (6) p6	0.0793	0.0035	0.267	0.010	1522	53	1543	66
Mnz_Loc (6) p7	0.0770	0.0034	0.259	0.010	1482	53	1499	64
Mnz_Loc (6) p8	0.0861	0.0039	0.305	0.012	1710	60	1669	72
Mnz_Loc (6) p9	0.0783	0.0035	0.258	0.011	1477	56	1522	66
Mnz_Loc (6) p10	0.0801	0.0036	0.270	0.011	1534	54	1557	67
Mnz_Loc (6) p11	0.0827	0.0037	0.272	0.011	1545	55	1605	69
Mnz_Loc (6) p12	0.0791	0.0036	0.267	0.011	1520	55	1538	67
Mnz_Loc (6) p13	0.0803	0.0036	0.263	0.010	1500	52	1560	67
Mnz_Loc (6) p14	0.0785	0.0035	0.260	0.010	1485	52	1527	65